Basin Research (2005) **17**, 83–108, doi: 10.1111/j.1365-2117.2005.00255.x

3D seismic interpretation of slump complexes: examples from the continental margin of Israel

Jose Frey Martinez,* Joe Cartwright* and Ben Hall†

**3DLab, School of Earth, Ocean and Planetary Sciences, Cardiff University, Cardiff, UK*
†BG-Group, Thames Valley Park Drive, Reading, UK

ABSTRACT

This paper uses three-dimensional (3D) seismic data from the continental margin of Israel (Eastern Mediterranean) to describe a series of slump deposits within the Pliocene and Holocene succession. These slumps are linked to the dynamics of subsidence and deformation of the transform margin of the eastern Mediterranean. Repeated slope failure occurred during the post-Messinian, when a clay-dominated progradational succession was forming. This resulted in large-scale slump deposits accumulating in the mid-lower slope region of the basin at different stratigraphic levels. It is probable that the slumps were triggered by a combination of slope oversteepening, seismic activity and gas migration.

The high spatial resolution provided by the 3D seismic data has been used to define a spectrum of internal and external geometries within slump deposits. Importantly, we recognise two main zones for many of the slumps on this margin: a depletion zone and an accumulation zone. The former is characterised by extension and translation, and the latter by complex imbricate thrusts and fold systems. Volume-based seismic attribute analysis reveals transport directions within the slump deposits, which are predominately downslope, but with subtle variations particularly at the lateral margins. Basal shear surfaces are observed to ramp both up and down stratigraphy. Slump evolution occurs both by retrogressive upslope failure, and by downslope propagation (out-of-sequence) failure. Slump anatomy and the combination of factors responsible for slump failure and transport are relatively poorly understood, mainly because of the limited 3D of outcrop control; hence, this subsurface study is an example of how improved understanding of the mechanisms and products can be obtained using this 3D seismic methodology in unstable margin areas.

INTRODUCTION

Submarine slump deposits are widely recognised from several continental margins and are an important component of many slope systems (Moore *et al*., 1976; Field *et al*., 1982; Bugge, 1983; Jansen *et al*., 1987; Barnes & Lewis, 1991; Field & Barber, 1993; Evans *et al*., 1996; Smith *et al*., 1999). Large-scale submarine slumping represents an important mechanism in shaping both active and passive margins whereby vast amounts of sediment are transported and redistributed into deep-water from an originally shallow-water setting.

Although slumping processes have been studied since the early 1920s, much of the research has been conducted on ancient slumps preserved in outcrop, and the incompleteness of the preserved slump bodies has been a persistent obstacle to a fuller, process-based analysis of the slump system (Locat & Lee, 2002; Strachan, 2002). In the last few decades, increasing use has been made of geophysical techniques such as two-dimensional (2D) seismic interpretation and sonar and multibeam imaging to characterise submarine slump deposits (e.g. Almagor & Wiseman, 1977; Prior & Coleman, 1978, 1979, 1982; Garfunkel *et al*., 1979; Nardin *et al*., 1979; Garfunkel, 1984; Moore *et al*., 1989, 1994a, b; Booth & O'Leary, 1991; Lee *et al*., 1991; O'Leary, 1991, 1993; Watts & Masson, 1995; Hampton *et al*., 1996; Lee *et al*., 1999; Bøe *et al*., 2000; McAdoo *et al*., 2000). Many valuable insights have been accrued from these approaches, but they are essentially 2D and suffer from many of the same limitations as the field-based analysis. In particular, 2D seismic data have inherent problems with the spatial aliasing of slump deposits and the geological structures within them. This has left many unresolved questions with regards to the detailed morphology, internal geometries and accurate areal extent of slump deposits, which limits our ability to construct more sophisticated kinematic and dynamic models for slumping.

Three-dimensional (3D) seismic technology offers a fundamentally novel method for investigations of both modern and subsurface slump deposits that promises to add significantly to our understanding of the mechanisms and results of slope instability processes. Modern,

Correspondence. Jose Frey Martinez, 3D Lab, School of Earth, Ocean and Planetary Sciences, Cardiff University, Main Building, Park Place, Cardiff CF10 3YE, UK. E-mail: jose@ocean.cf.ac.uk

high-resolution 3D seismic surveys are now acquired on many continental margins for hydrocarbon exploration purposes, and often in areas that are or have been prone to slope failure. The remarkable high spatial resolution that 3D seismic data provides (tens of metres in all three dimensions) can thus be used to define both the full areal extent and the external and internal morphology of submarine slump deposits to a high degree of precision in a way that cannot be achieved with any other combination of methods.

The principal aim of this paper, therefore, is to illustrate the potential for 3D seismic interpretation of slump systems by describing the geometry and distribution of a suite of slump deposits from the post-Messinian continental margin of Israel. This area is ideal for such an analysis because it contains many well-preserved examples of both deeply buried and shallow slump deposits. A secondary aim is to examine the stratigraphic evolution of slumping and its role in the overall development of the margin. The paper commences with an overview of the geological setting and a description of the stratigraphic context of the slump deposits in the study area. The main arguments are subsequently developed through detailed 3D seismic analysis focused on two representative case studies.

REGIONAL TECTONO-STRATIGRAPHIC CONTEXT

The study area is located offshore Israel, and comprises the continental margin that bounds the onshore platform of Israel with the oceanic lithosphere of the Eastern Mediterranean Sea (Fig. 1a). This margin is situated in an active tectonic setting at the zone of interaction between the Anatolian, African and Arabian plates (Fig. 1a). Its early development is related to a sequence of rifting events from the Early Permian to the Middle Jurassic, during the first stages of disintegration of Pangea (Garfunkel, 1998). Throughout this period, opening of the Tethys Ocean caused rifting to the north of the African plate resulting in break-up of the extensive shallow-water carbonate platform that had dominated the palaeogeography of the area. The subsequent continental break-up that led to the initiation of spreading in the eastern Mediterranean region resulted in the formation of a passive continental margin from the end of the Middle Jurassic (Garfunkel & Derin, 1984). During this period, high-energy carbonate platforms bordered by deep-water basins developed until the Late Cretaceous (Garfunkel, 1998).

In the Late Cretaceous, a change in the relative motion of the African plate with respect to the Eurasian plate led to

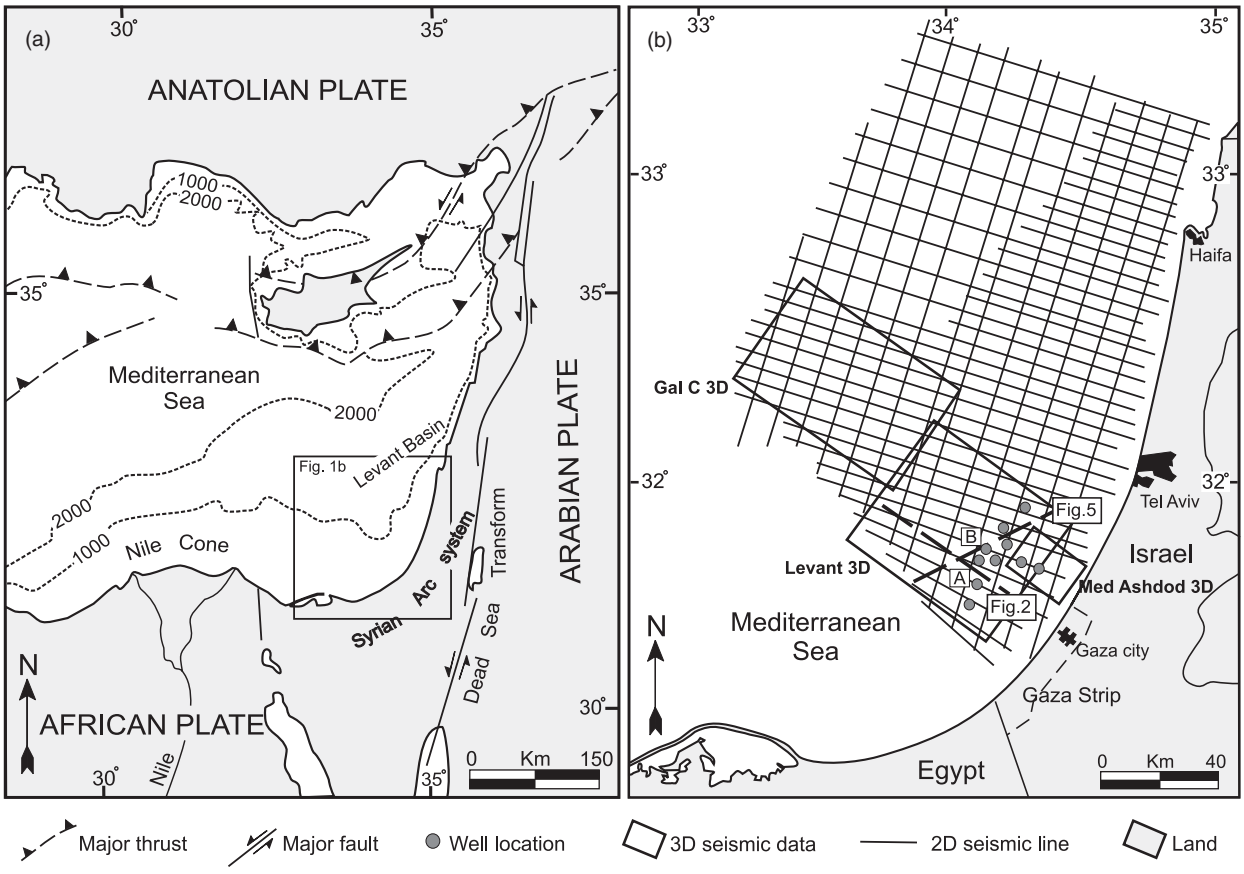

Fig. 1. (a) Geological sketch of part of the Eastern Mediterranean showing the main structural elements. The box marks the approximate location of the study area. Modified from Garfunkel (1998). (b) Location map for the study area showing the 2D and 3D seismic database used in the study and locations of key exploration wells (A and B mark the location of the Gaza Marine-1 and the Or-South-1S wells, respectively). Dashed lines indicate the location of seismic profiles (Figs 2 and 5).

a compressive stress-regime and the formation of the Syrian Arc system (Figs la and 2; Ben-Avraham, 1989; Tibor & Ben-Avraham, 1992; Eyal, 1996). The Late Cretaceous carbonate platform was drowned and pelagic sedimentation prevailed until the Oligocene (Druckman *et al*., 1995).

During the Miocene, the shelf area experienced localised tectonic uplift and became intermittently emergent. Conversely, the slope and basin areas continued to subside (Buchbinder & Zilberman, 1997). As a result, several submarine canyons (e.g. el-Arish, Afiq and Ashdod) that initially incised during the Oligocene (Druckman *et al*., 1995) extended to the shelf through headward erosion (Buchbinder & Zilberman, 1997). These canyons subsequently played an important role in the overall progradation and stability of the margin. Marine sedimentation was limited to the slope and basin areas, where the submarine canyons provided a conduit for fine-grained siliciclastics to be deposited directly onto the basin floor.

In the Late Miocene, the evolution of the margin was greatly influenced by the desiccation of the Mediterranean Sea during the Messinian Salinity Crisis (Tibor & Ben-Avraham, 1992). An extensive subaerial unconformity formed along basin margins while thick evaporitic deposits (Mavqiim Formation) were laid down over the former basin floor (Hsü *et al*., 1978; Montadert *et al*., 1978) (Figs 2 and 3).

During the Pliocene, the vertical tectonic movement reached its peak (Almagor, 1993) and a major transgression submerged the exposed Upper Miocene shelf (Buchbinder & Zilberman, 1997). Clay-rich marls, sandstones and claystones deposited in the slope and basin areas (Yafo Formation; Fig. 3). During this period, the gross configuration of the margin constituted a strongly aggradational system, with sigmoidal clinoforms linking shelf to slope (Fig. 2). Several episodes of large-scale slumping and gravitational tectonics (e.g. Almagor, 1980, 1984, 1986; Garfunkel, 1984; Garfunkel & Almagor, 1985 and 1987) alternated with periods of hemipelagic deposition.

During the Pleistocene, global eustatic sea-level oscillations and local vertical tectonic movements resulted in repeated advances and retreats of the shoreline. Consequently, interbedded sands, clays and marls accumulated in the shelf under alternating terrestrial and marine conditions (Sivan *et al*., 1999) (Herfer Formation; Fig. 3). A Holocene transgression resulted in sedimentation of silt-rich clays over the present-day continental terrace. The gross configuration of the margin was similar to that in the Pliocene, i.e. a strongly aggradational system affected by slumping and gravitational tectonics (Fig. 2).

DATABASE AND METHODOLOGY

Conventional 2D and high-resolution 3D seismic data represent the main source of information for this study. Wireline logs (γ-ray, sonic and resistivity) and commercial stratigraphic reports, mainly based on cuttings analyses, were available from 10 exploration wells located in the study area (Fig. 1b). The regional 2D seismic database of offshore Israel used for this study comprises approximately 6000 km in a 10 km by 10 km grid (Fig. 1b).

Three 3D seismic surveys were available for this study (Med Ashdod, Levant and Gal C) and constitute the high-resolution data (Fig. 1b). The total 3D seismic coverage amounts to 3200 km^2, extending from the shelf to the deep basin areas. These datasets, in comparison with the 2D seismic data, allow considerably better seismic–stratigraphic resolution because of improved acquisition and processing methods. All three surveys were acquired with an in-line trace interval of 6.25 m and a cross-line spacing of 25 m. Final processing yielded a time-migrated 12.5 m by 12.5 m grid (i.e. 6400 bin cells km^2). The dominant frequency of the seismic data varies with depth, but it is approximately 50 Hz at the base of the Pliocene. Vertical and lateral resolutions are estimated to be about 10 and 100 m, respectively. An average seismic velocity of 2000 m s^{-1} has been assumed within the first 2.5 s of the 3D datasets. This velocity is derived from the check-shot measurements made from the Gaza Marine-1 exploration well.

Firstly, regional mapping at different stratigraphic levels on the 2D and 3D seismic datasets was undertaken to identify and map the main slump deposits. Secondly, a detailed seismic–stratigraphic framework was established by tying the 3D seismic interpretation of the slumps and the intervening sedimentary units with litho- and biostratigraphic information from the 10 wells located in the study area (Fig. 1b). Detailed 3D seismic mapping of slump deposits was undertaken by correlating the base and the top of the selected slumps. Subsequently, flattened horizontal coherence slices and seismic attribute extractions were generated in representative areas to analyse the external seismic geometry of individual slump deposits and to examine their transport directions and internal fabrics.

RECOGNITION OF SLUMP DEPOSITS ON 3D SEISMIC DATA

There is considerable overlap and confusion in the literature in the usage of the terms 'slump' and 'slide'. In this paper, slumps are defined after Stow (1986) as downslope movements of sediments above a basal shear surface where there is significant internal distortion of the bedding. Mulder & Cochonat (1996) divided slump deposits into two end members: simple and complex. Simple slump deposits are those in which slumping operates as an isolated and single event and does not generate other significant failures (e.g. Knebel & Carson, 1979). In contrast, complex slump deposits are those in which the motion of the main sedimentary block leads to instability of neighbouring areas, and the volume of such induced successive events is similar to the volume of the initial slump (e.g. Lewis, 1971; Barnes & Lewis, 1991). All the examples of slump deposits presented in this paper belong to this latter complex type.

Fig. 2. Regional dip seismic section through the continental margin of Israel (see Fig. 1b for location). This seismic profile illustrates the post-Cretaceous configuration of the study area. Note the presence of an extensive unconformity and a thick deposit of evaporites resulting from the Messinian Salinity Crisis. Listric shore parallel growth faults are related to gravity-driven deformation of the Pliocene–Holocene continental margin and to salt tectonics.

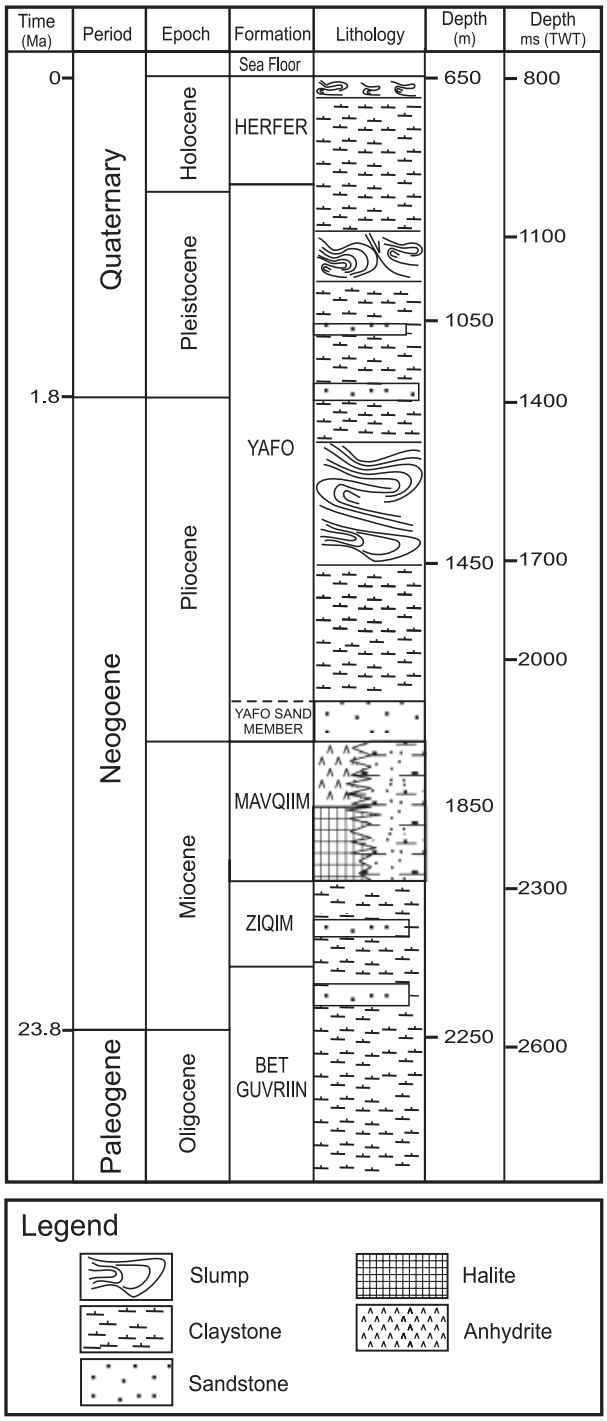

Fig. 3. Generalised chrono-stratigraphic and lithological scheme of the post-Eocene continental margin of Israel. The lithological column is based on unpublished well reports.

Slump units are recognised on seismic data using some simple criteria established from a number of previous studies (Embley & Jacobi, 1977; Woodcock, 1979; Embley, 1980; Field *et al*., 1982; Prior & Coleman, 1982; Prior *et al*., 1984; Bugge *et al*., 1987; Jansen *et al*., 1987; Kenyon, 1987; Normark & Gutmacher, 1988; Trincardi & Normark, 1989; Evans *et al*., 1996; Hampton *et al*., 1996; Smith *et al*., 1999; Lee *et al*., 2002). Most important of these is the recognition of a body that is characterised internally by chaotic or highly disrupted seismic facies that covers a large enough area to be identifiable as a discrete stratigraphic unit (Fig. 4). Scale is thus important because of the limitations of seismic resolution: if a slump is so small that it is beyond vertical and horizontal seismic resolution, then clearly it is impractical to interpret it as a slump *per se*. The external geometry of the chaotic unit is therefore a critical parameter allowing slump masses to be distinguished from other types of depositional units that often exhibit chaotic seismic facies, such as canyon fills, channel fills or talus wedges as, for example, described by Brown & Fisher (1977).

The basal shear surface is perhaps the most critical aspect leading to the correct identification of a slumped mass. Discrete slump events are usually associated with specific basal shear surfaces (e.g. Farrell, 1984), so an accurate definition of these surfaces offers a potential method for discriminating between successive slump events within a slump complex. The basal shear surface is identified in a similar way to unconformities, i.e. by termination of stratal reflections (Fig. 4). This is aided by the often significant contrast between the chaotic facies of the slump and the much more continuous seismic facies of the undeformed slope deposits (Fig. 4). Over much of the area of a slump deposit, the basal shear surface forms a continuous plane that dips parallel to the underlying strata. However, this surface may locally ramp up and down the stratigraphy to form a step-like geometry. Near the headwall, the basal shear surface exhibits a listric, concave upward appearance, cutting the upslope strata (Fig. 4a). Approaching the toe (*sensu* Varnes, 1978), the basal shear surface generally ramps upwards cutting into the downslope strata to form a frontal ramp (Fig. 4b).

The top of the slumped unit is simply defined by correlating the boundary between the chaotic or disrupted facies and the more continuous overlying strata. In the event that the depositional system following the slump episode is itself comprised of discontinuous or chaotic seismic facies, this boundary can be very difficult to interpret with accuracy. However, on many slopes where slumps occur, hemipelagic deposits tend to be the first sediments to drape a slump mass, and these are generally highly continuous, and easily separated from the underlying slump (Fig. 4b). In many cases in the study area, the top surfaces of slump bodies correspond to irregular and mounded surfaces with localised depressions where it is common to find onlap or downlap of the overlying units (Fig. 4).

STRATIGRAPHIC CONTEXT OF SLUMP DEPOSITS IN THE STUDY AREA

Using the diagnostic criteria described in the previous section, over 40 slump complexes have been identified within the post-Messinian succession of the southern Israeli continental margin. It is apparent that there are distinct regions of the margin where these slump complexes are concentrated; in particular the presence of a slump deposit influences the position of succeeding slumps. This

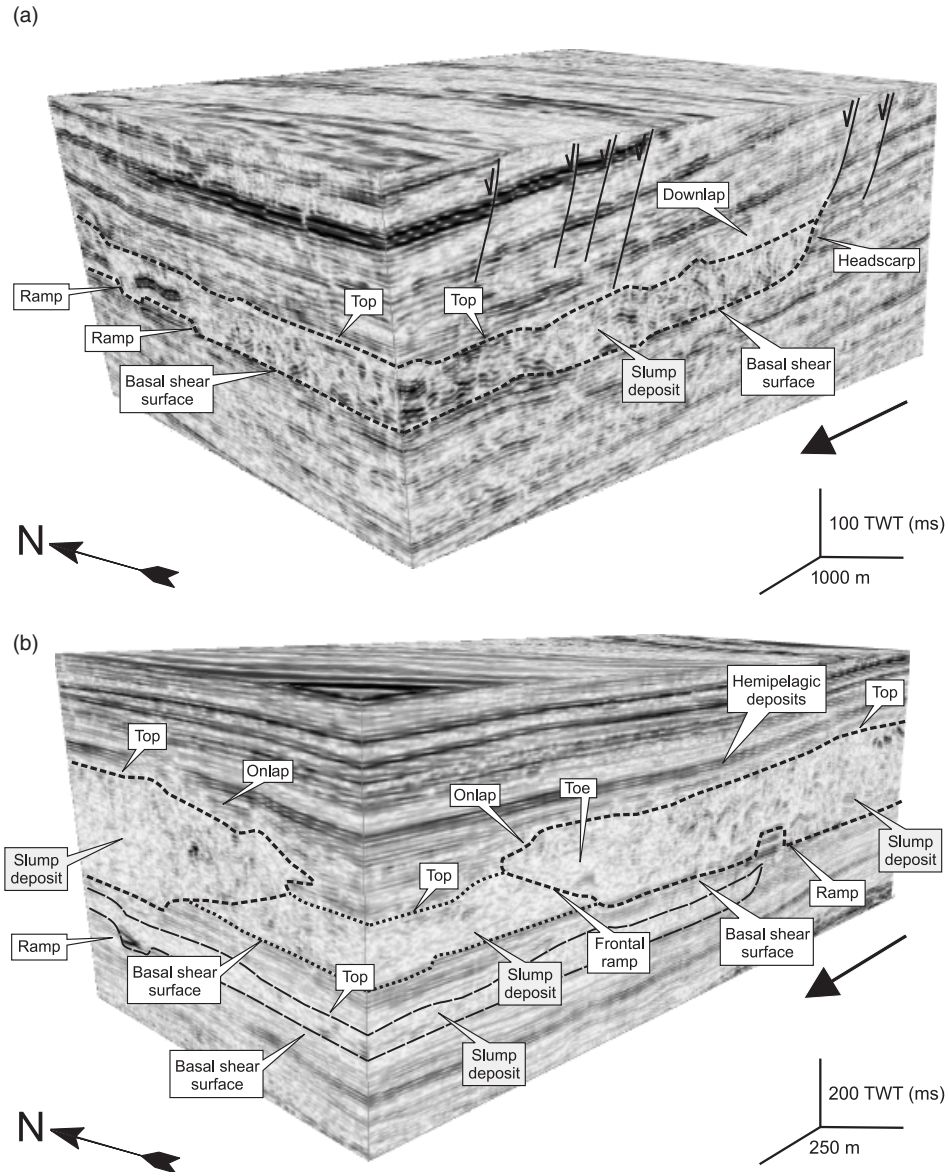

Fig. 4. 3D visualisation of representative slump deposits in the study area. Slump masses form intervals of disrupted and chaotic seismic facies enclosed by the basal shear and the top surfaces. Black arrows mark the main downslope direction of movement. (a) 3D seismic block showing the upslope parts of a slump deposit. Note the listric character of the basal shear surface towards the headscarp and the irregular morphology of the top surface. Presence of downlap from the overlying strata. (b) 3D seismic volume showing the downslope parts of a slump deposit. Note the presence of other older slump deposits being intersected. The basal shear and the top surfaces mark the limits between the chaotic seismic facies within the slump deposits and the continuous reflections of the outer undeformed strata. Note the presence of a frontal ramp towards the toe of the slump mass.

section describes these gross stratigraphic relationships using a combination of regional 2D and detailed 3D seismic interpretation.

The post-Messinian succession of the southern parts of the study area has been divided into three seismic–stratigraphic units as a basis for discussing the distribution of slump deposits (Fig. 5). These three units (T30, T20 and T10) correspond approximately to the Pliocene, the Early–Late Pleistocene and Late-Pleistocene-Recent, respectively. The Plio–Pleistocene boundary is based on biostratigraphic data tied to the seismic data from 10 exploration wells, and is a remarkably consistent seismic reflection throughout the basin. The boundary between the upper two units is not constrained by biostatigraphy, but it is assumed to be of Late Pleistocene age based on the average thickness of the upper unit and an extrapolation of sedimentation rates from the exploration wells. The areal distribution of the main slump complexes within these three units as mapped within the 3D seismic data sets is summarised in Fig. 6.

Unit T30

Unit T30 consists of a ca. 750 m thick accumulation of mainly fine clastic sediments that are part of a prograding and aggrading slope wedge (Fig. 5). The basal part of this unit is devoid of any slumps, and consists of sandstones interbedded with thin glauconitic claystones and marls interpreted as basin floor turbiditic fan deposits (Yafo Sand Member; Fig. 5). The seismic character of the Yafo Sand Member is expressed as a package of high-frequency, continuous, high-amplitude seismic reflections that are restricted to the areas underlain by the Afiq and el-Arish canyons. Overlying this is a ca. 700 m thick package consisting mainly of continuous high-amplitude reflections representing the main phase of hemipelagic and turbiditic

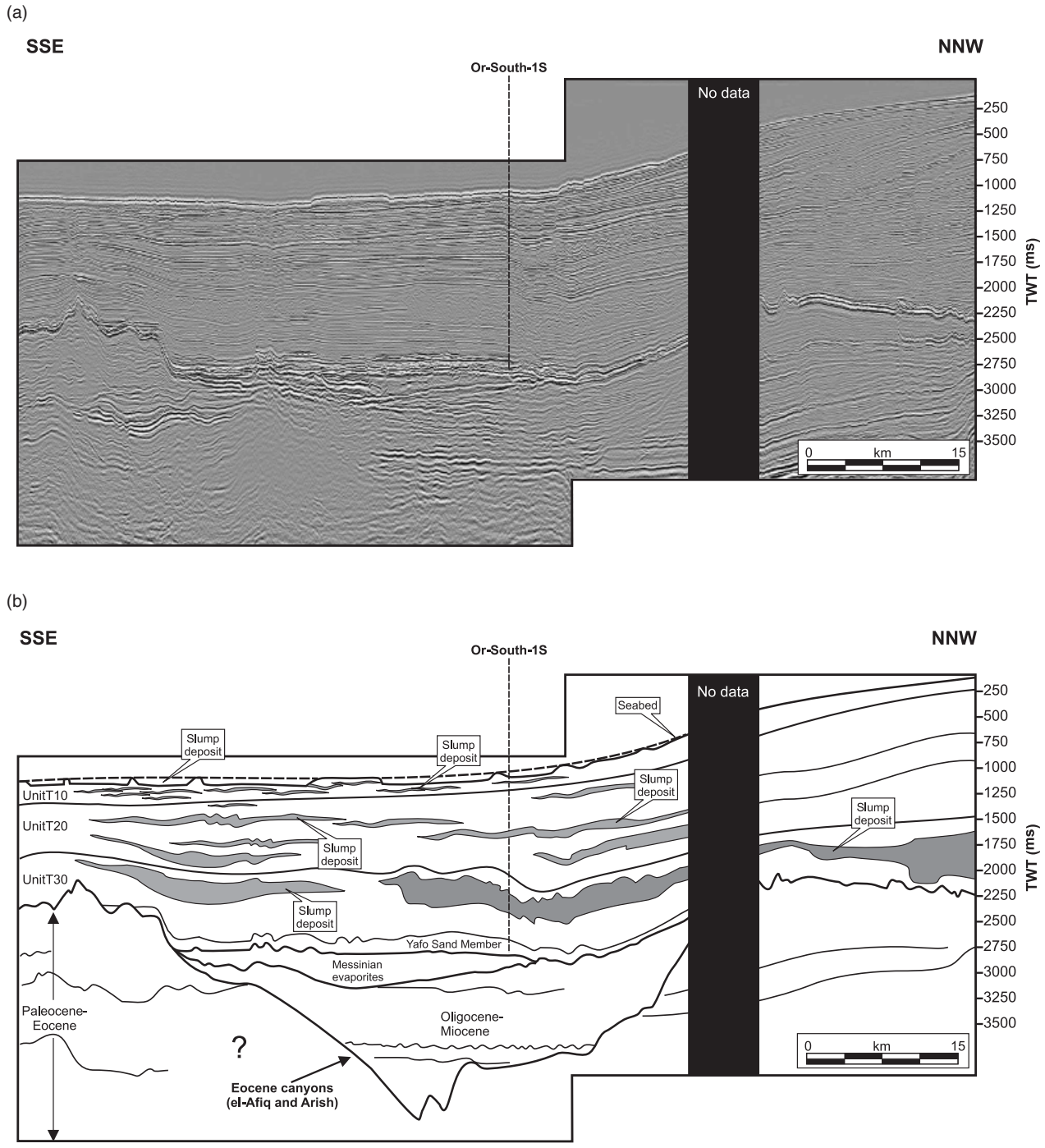

Fig. 5. Seismic section (a) crossing the central parts of the Levant 3D area (see Fig. lb for location) and (b) interpretation showing the stratigraphic context of slump deposits in the study area. Shaded areas correspond mainly to simple slump deposits. Note that there is a concentration of slump deposits in the locations overlying pre-Messinian canyons. Slumps increase in number and decrease in size upwards (see text for discussion).

slope wedge deposition, with strongly aggradational reflection configurations (Fig. 5).

Within the upper part of Unit T30 a major slump complex extending almost continuously along the margin is identified (Figs 5 and 6a). This slump complex comprises a minimum of three large-scale slump deposits and creates the biggest seismic stratigraphic break not just on Unit T30 but also within the entire post-Messinian continental margin of Israel. It involves up to 350 m of sediments and covers most of the slope region of the continental margin of Israel. In volume, this slump complex consists of up to ca. 1000 km^3 of Pliocene sediments, and affects, therefore, up to ca. 30% of the total Pliocene sedimentary column. This slump complex is herein termed as the Israel Slump Complex (ISC) and it is described in greater detail in a later section.

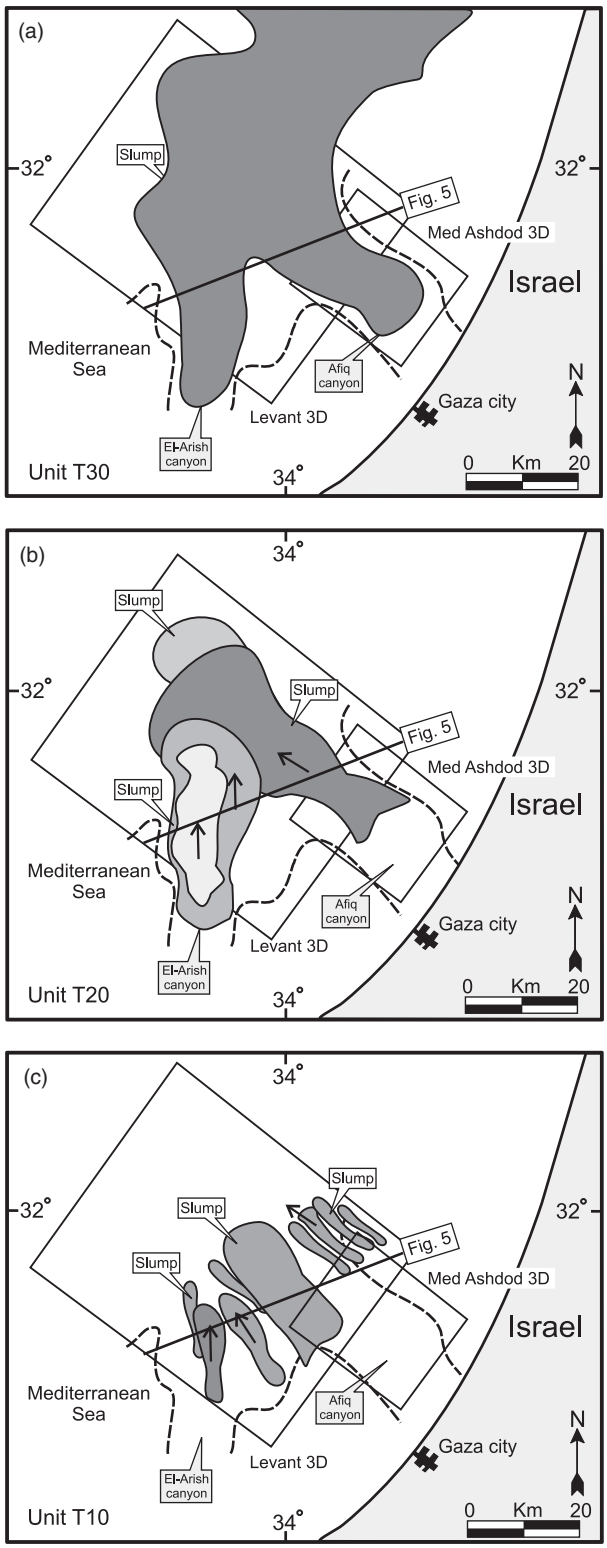

Fig. 6. Maps showing the areal distribution of slump deposits within the 3D seismic surveys in the three seismic–stratigraphic units defined in the text. Arrows indicate the interpreted directions of movement. Dashed lines represent the flanks of the Afiq and el-Arish canyons. (a) Areal distribution of a major slump complex within Unit T30. (b) Areal distribution of slump deposits within Unit T20. Note the concentration of slump deposits in the areas underlain by the Arish and el-Arish canyons. (c) Areal distribution of slump deposits within Unit T10.

Unit T20

Unit T20 consists of a ca. 1000-m thick interval of continuous, moderate-to-high amplitude seismic reflections defining a major aggradational slope wedge with dominantly sigmoidal clinoform geometries (Fig. 5). Shallow to deep-marine claystones and limestones that locally alternate with sandstones, siltstones and marls form the bulk of this unit. Many small-to-moderate-sized slump bodies (typically < 100 m thick) are mapped within this interval in an upper-mid slope position. A volumetric analysis reveals that up to ca. 400 km^3 of Pleistocene sediments are affected by slump units in Unit T20. This figure represents nearly half of the slump volume of that in Unit T30. However, the number of individual slump complexes in Unit T20 is over 15, which is considerably higher than the small number computed for Unit T30.

The areal distribution of slump complexes within Unit T20 is particularly interesting. In the vertical sense, slumps form two sets of stacked bodies that are commonly interbedded with undisturbed, continuous and well-bedded seismic reflections interpreted here as hemipelagic slope sediments (Fig. 5). This distribution suggests that the presence of a slump deposit influences the vertical position of succeeding slumps and that compensational stacking does not apply. The lateral distribution of slumps within Unit T20 is also interesting as they are restricted to areas underlain by the Afiq and el-Arish canyons (Figs 5 and 6b). This lateral distribution suggests some sort of intrinsic control for these areas to act as major conduits for the generation of slump complexes.

Unit T10

Unit T10 is the uppermost 100–200 m of the post-Messinian section consisting of mainly fine-grained clastic sediments deposited in an aggrading sigmoidal clinoform configuration (Fig. 5). Piston core testing carried out in the study area (e.g. Almagor & Wiseman, 1977; Almagor & Schilman, 1995) shows that the present-day shelf and slope sediments consist mainly of normally consolidated dark grey claystones (up to 75%) comprising 60–80% montmorillonite, 20–40% kaolinite, 1–15% illite, and very low carbonate content. Geotechnically, the sediments are characterised by bulk density of $\rho = 1.44–1.51\ g\ cm^{-3}$, water content of 90–110%, liquid limit of 70–95%, plasticity index of 45–65%, effective angles of internal friction of 21–29° and total angles of internal friction of 14–17° (Frydman *et al.*, 1982).

Numerous slump bodies have been mapped within Unit T10. These are particularly well imaged on the present day seabed as described in the following section (Fig. 7). The slump bodies are distributed over the entire Upper Pleistocene-Recent section forming complexes that extend from the shoreline break to the base of slope (Figs 6c and 7). The dimensions of these slump complexes are considerably smaller than those in Units T20 and T30, typically with surface areas of ca. 80 km^2. However, their total

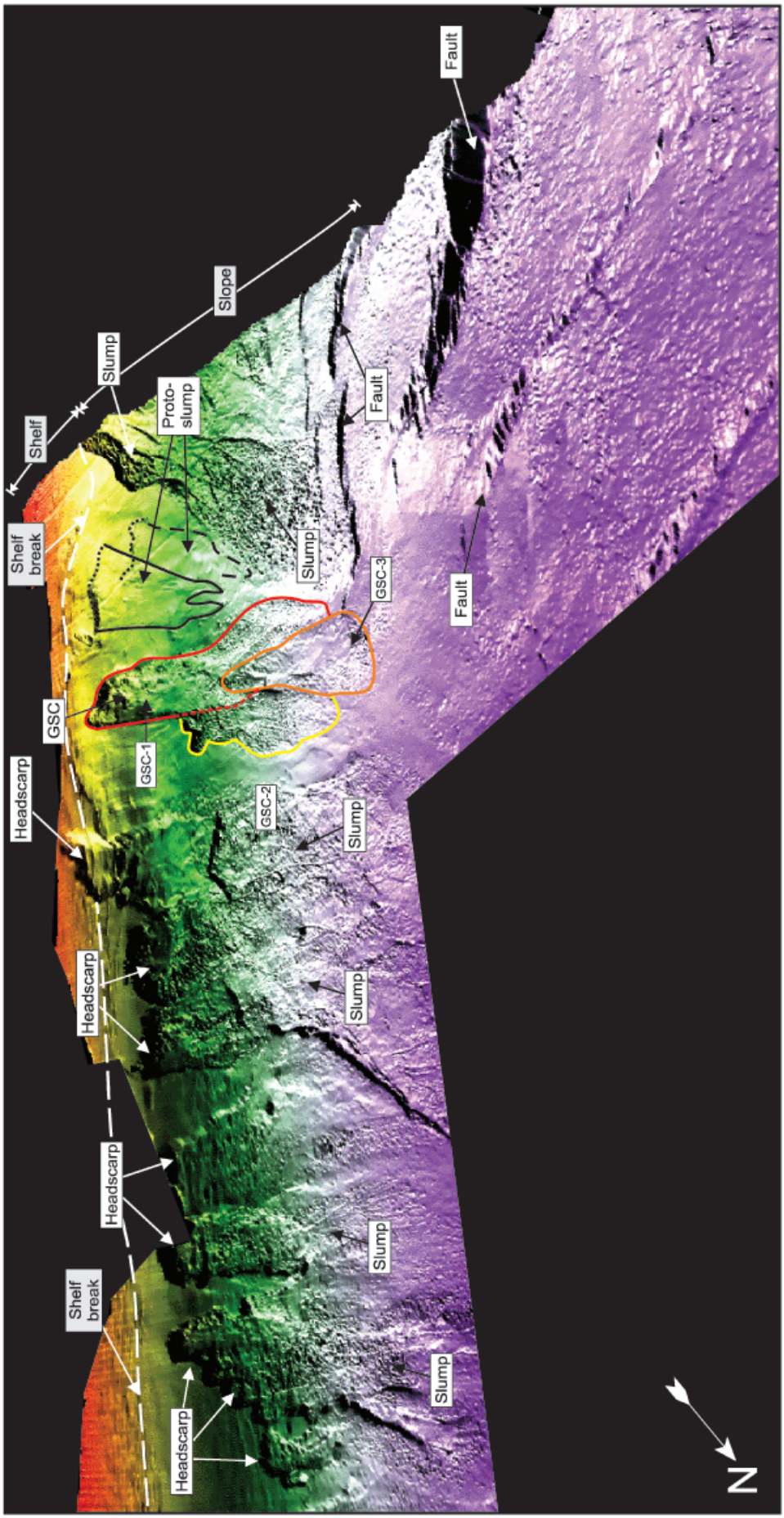

Fig. 7. 3D perspective view of the present day seabed in the Levant 3D area. Note the presence of several slump complexes covering the slope region. These form arrays of elongated slump deposits extending from the shelf to the base of slope areas. Note the presence of headscarps and secondary crown-cracks. Inset shows the Gaza Slump Complex (marked by GSC).

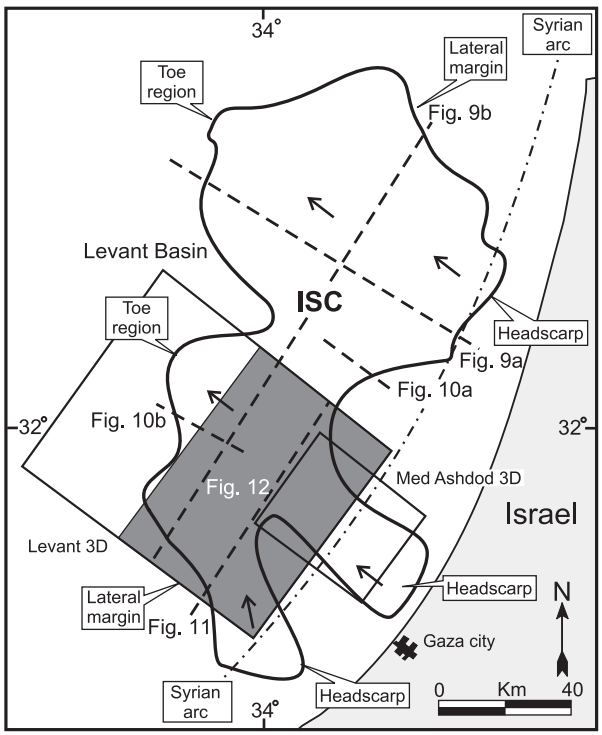

Fig. 8. Map of the Israel Slump Complex (ISC) showing its areal extension. Note its enormous areal extent (ca. 4800 km^2). The dashed line (parallel to the coastline) marks the general trend of large tectonic structures from the Syrian Arc system. Arrows indicate the gross transport direction of the slump mass. Seismic sections (indicated with thick dashed lines) are used to illustrate the regional seismic appearance of the ISC (Figs 9–11). The area where detailed 3D seismic interpretation has been undertaken is indicated by the shaded box (Fig. 12).

number (ca. 25) is significantly higher to that of Units T30 and T20 (ca. 1 and ca. 15, respectively).

Within Unit T10, one slump complex extends almost continuously from the shelf-break to the base of slope areas. This consists of a composite of three different slumps that form an intricate cross-cutting array. In this paper, it is referred as the Gaza Slump Complex (GSC in Fig. 7) and will be described in detail in the following section.

DETAILED 3D MAPPING OF SLUMPS

Two slump complexes display typical characteristic on 3D seismic data and are described here. The first case study is of the ISC of Early Pliocene age, which is remarkable in several aspects, not least of which is its enormous volume (ca. 1000 km^3), placing it amongst the world's largest slump deposits (i.e. Storegga Slide; Bugge, 1983). The second is of the much smaller GSC of Late Pleistocene/Holocene age, which is expressed at the present seabed. This allows for a much higher resolution of surface topography, comparable with modern multibeam bathymetry data. The combination of surface imagery with the vertical seismic profiles allows for very detailed morphometric analysis that has revealed a complex kinematic history.

The ISC

The ISC is a large-scale buried slump complex that extends over an area of 4800 km^2 (Figs 8 and 9). The ISC affects in excess of 300 m of deep-water claystones from the Upper Pliocene and has a volume of up to ca. 1000 km^3. These enormous values make the ISC comparable with some of the largest documented examples of submarine mass-wasting deposits (e.g. Woodcock, 1979; Bugge, 1983; Bugge *et al*., 1987; Jansen *et al*., 1987; Kenyon, 1987; Evans *et al*., 1996; Hampton *et al*., 1996).

The ISC is positioned at the transition between two distinct morpho-structural zones: the Syrian Arc system and the Levant basin (Fig. 8). The first zone underlies the upslope parts of the ISC, where the Pliocene margin consists of steep slopes with maximum gradients of ca. 6° (Fig. 9a). The second zone lies beneath the downslope and central parts of the ISC. Here, the undisturbed Pliocene strata dip at ca. 1° and are underlain by thick (> 800 m) deposits of Messinian evaporites (Fig. 9a). The gross transport direction of the ISC is west-northwest.

Seismic character of the ISC

The limitations of the coarse regional grid of the 2D seismic data preclude any accurate mapping of the northern and central parts of the ISC. Therefore, detailed mapping and seismic analysis was undertaken in its southern parts where 3D seismic data were available (Fig. 8).

The seismic expression of the ISC is recognisable as a zone of chaotic to discontinuous seismic reflections bounded above, below and laterally by continuous strata of Unit T30. In the downslope direction (Fig. 9a), the ISC is seen as a continuous package that extends for ca. 150 km along the continental margin. On strike profiles (Fig. 9b), the ISC forms an approximately rectangular body dominated by a chaotic seismic facies sharply in contrast with the more continuous seismic reflections from the undisturbed strata. The ISC shows significant variations in thicknesses that are spatially related to large-scale discordances at its basal shear surface (Fig. 9b).

Headscarp. The headscarp of the ISC is located between 2- and 20 km offshore the present day coastline of Israel (Fig. 8). In plan view, it is mapped as an irregular boundary, with three main salients suggesting that the ISC consists, at least, of three major slump bodies (Fig. 8). Unfortunately, the lack of high seismic resolution data has precluded a more detailed analysis of their spatial distribution and chronology. On seismic profiles, it is recognisable as a concave upwards surface that separates the chaotic seismic facies of the slump body from the undisturbed surrounding strata (Figs 9a and 10a). Its upper tip is generally between 200 and 300 m above the level of the basal shear surface and has a gradient ranging from ca. 2° in the southern parts of the ISC to ca. 15° in the north. Near the headscarp, the top of the ISC is depressed with respect to the undeformed region of the slope and it

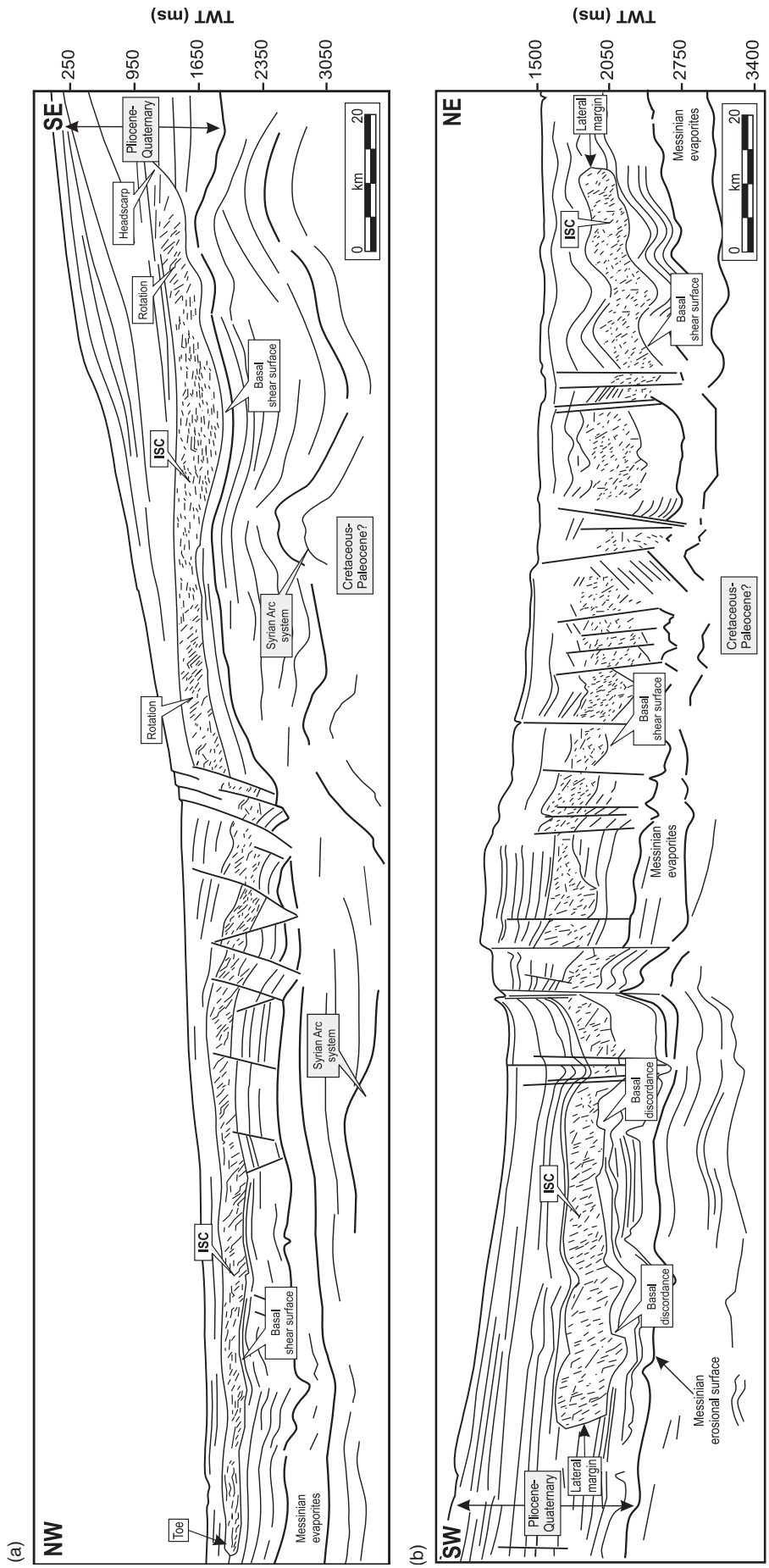

Fig. 9. (a) Dip geo-seismic section through the continental margin of Israel (see Fig. 8 for location). The profile images the Israel Slump Complex (ISC) as a package of chaotic seismic facies within the Lower Pliocene slope system. Reflections within the ISC exhibit local rotation away from the headscarp. The toe region forms an abrupt change from chaotic facies (ISC) to continuous facies (base of slope units). Note the presence of salt-detachment growth faults deforming the ISC. (b) Strike geo-seismic section through the continental margin of Israel (see Fig. 8 for location). The profile images the ISC as a continuous body extending from the southern to the northern parts of the margin. The lateral margins of the ISC appear as limits to the chaotic facies within the slump mass. Note the presence of discordances in the basal shear surface and faults deforming the slump mass.

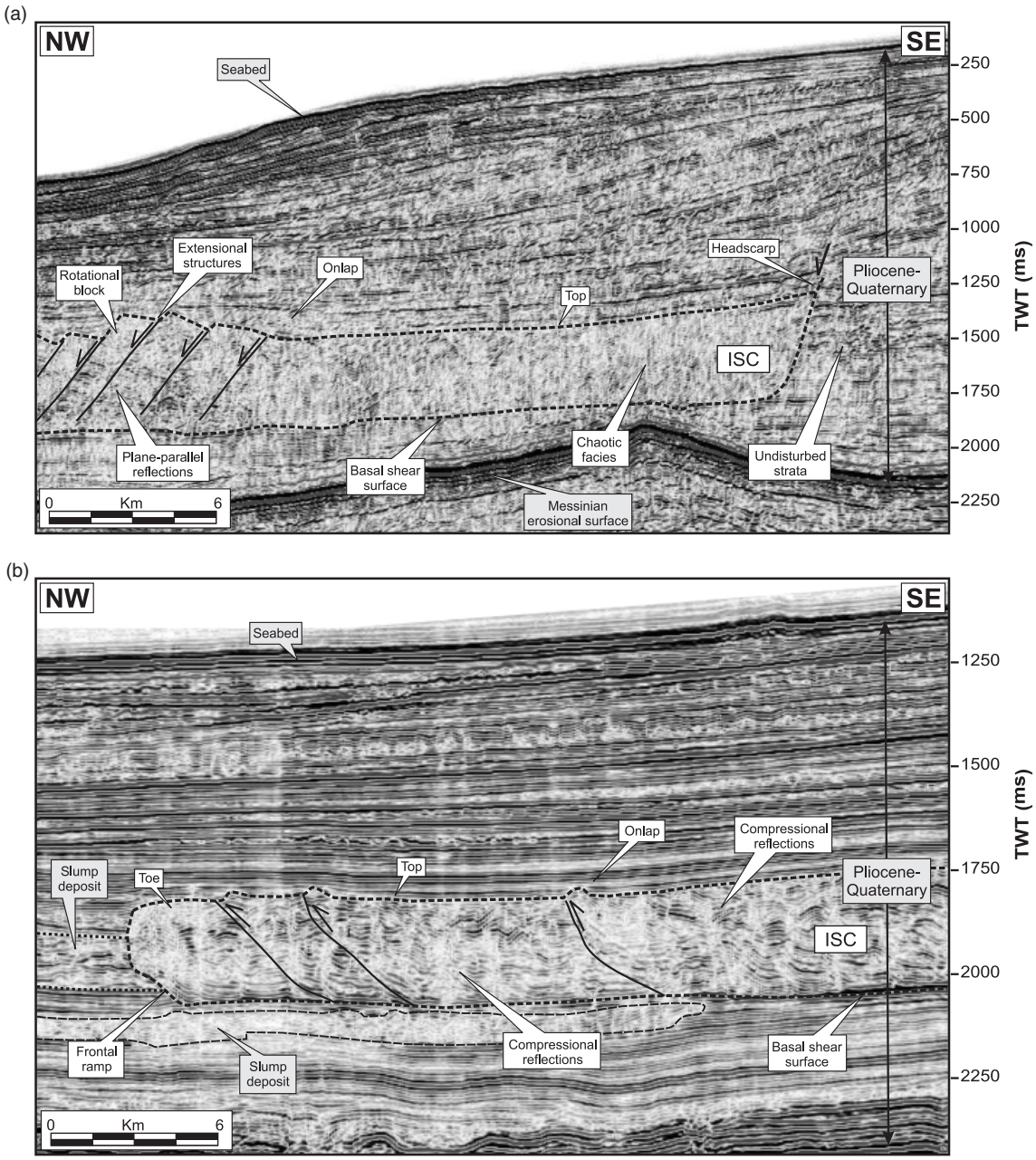

Fig. 10. Seismic profiles along the Israel Slump Complex (ISC). (a) 2D seismic profile in the upslope parts of the ISC (see Fig. 8 for location). The headscarp forms a steeply dipping interface forming the updip boundary between the chaotic seismic facies within the slump body and the continuous reflections of the upper slope. Clear onlap of the headscarp by post-slump sediments is observed. (b) 3D seismic profile through the toe region of the ISC (see Fig. 8 for location). The toe region appears as the downslope boundary between chaotic seismic facies of the ISC and the continuous reflections of the base of slope. Note the presence of a clear frontal ramp and the slump mass being buttressed against the downslope strata. Older slump deposits appear affected by the ISC.

is onlapped by post-slump deposits, suggesting that the ISC is thinned relatively to the pre-slump slope template (Fig. 10a).

Toe. The toe of the ISC is positioned between 100 and 140 km offshore Israel (Fig. 8). On downslope seismic profiles, it is very well constrained by an abrupt change from the chaotic seismic facies within the ISC to the continuous seismic reflections at the base of the slope areas (Figs 9a and 10b). In some parts of the toe region, the ISC is seen to affect various intervals of chaotic seismic facies interpreted as older slump deposits (see Fig. 10b).

In the toe region, the basal shear surface steepens dramatically to form a frontal ramp seen as a boundary between the chaotic seismic facies within the ISC and the continuous seismic facies outside. In this region, the slump mass appears buttressed against the outer continuous strata. Only locally developed evidence of slumped material overlying the downslope strata are observed.

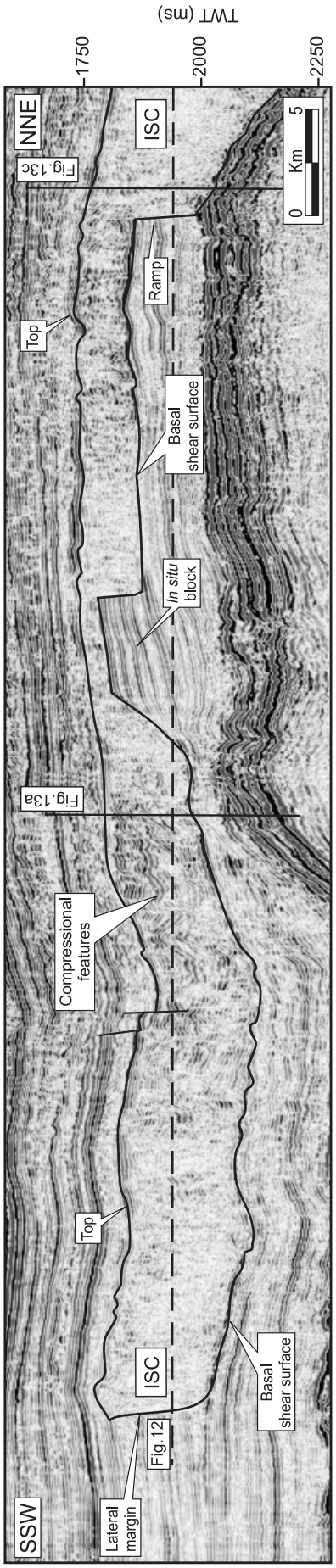

Fig. 11. 3D seismic profile across the Israel Slump Complex (ISC) (see Fig. 8 for location). Note the intensively chaotic seismic facies of the internal parts of the ISC bounded above and below by the top and basal shear surface, respectively. A lateral flank of the ISC forms a highly steep ramp separating chaotic for continuous seismic facies. Note the presence of a ramp indenting the basal shear surface and a block of undisturbed reflections within the ISC (see text for discussion). A horizontal coherence-slice (Fig. 12) and three seismic profiles (Fig. 13) are used to further illustrate the internal geometry of the ISC.

However, the volumes involved are in no case consistent with the dimensions involved by the ISC. In the area surrounding the toe, the top of the slump mass is elevated with respect to its lateral correlative reflection within the undeformed region of the slope and it is onlapped by post-slump deposits (Fig. 10b). These relationships suggest that the ISC is thickened relatively to the pre-slump slope template.

Lateral margins. The lateral margins of the ISC are only approximately constrained by the limits of the seismic grid in the study area. However, these are still recognisable on strike-oriented seismic profiles as abrupt lateral limits between the highly chaotic seismic facies within the ISC and the outer undeformed strata (Figs 9b and 11). Steep lateral ramps of the basal shear surface are observed along most of the margins abutting against the undeformed slope sediments (Figs 9b and 11). Although significantly steeper, these lateral ramps are similar in geometry to the frontal ramps observed at the toe of the slump body (e.g. Fig. 10b).

Internal geometry. The seismic character of the ISC is dominated by chaotic facies. However, there is sufficient coherence of individual intra-slump seismic reflections to allow local recognition and mapping of deformational features. These are particularly well imaged on the 3D seismic data, but can also be seen on 2D seismic profiles wherever the quality resolution of the data permits.

Throughout the upslope region of the ISC, the internal geometries generally consist of plane-parallel and laterally continuous reflections that are affected by extensional structures (e.g. listric normal faults). On seismic profiles, these are approximately parallel to the headscarp and create a series of tilted downslope rotational blocks (Fig. 10a).

The dominant internal seismic character within the downslope region of the ISC is significantly different to the upslope region (Figs 9b and 10b). Highly deformed and discontinuous seismic reflections are seen to be affected by compressional structures that contribute to a substantial thickening of the downslope parts of the ISC (e.g. thrusts and folds, Fig. 10b). The thrust systems are detached from the basal shear surface and ramp up to deform the upper surface of the ISC, such that localised mounded topographies and onlapped depressions are created (Fig. 10b). Flattened horizontal coherence slices show these thrust systems as concentric arcs of ridge-like structures extending in a gross downslope direction (Fig. 12). These are largely developed towards the toe region of the ISC and in areas where the basal shear surface shows significant topographic relief. On seismic profiles, their typical structural configuration is of an imbricated series of closely spaced thrusts (ca. 500–1000 m) with small thrust propagation folds developed at the thrust tips (Fig. 13). The average thrust displacement is of the order of 50–100 m, as measured on correlative markers within the slump body, and a typical degree of shortening expressed in the imbricate thrust set is of the order of 10%. This value of shortening

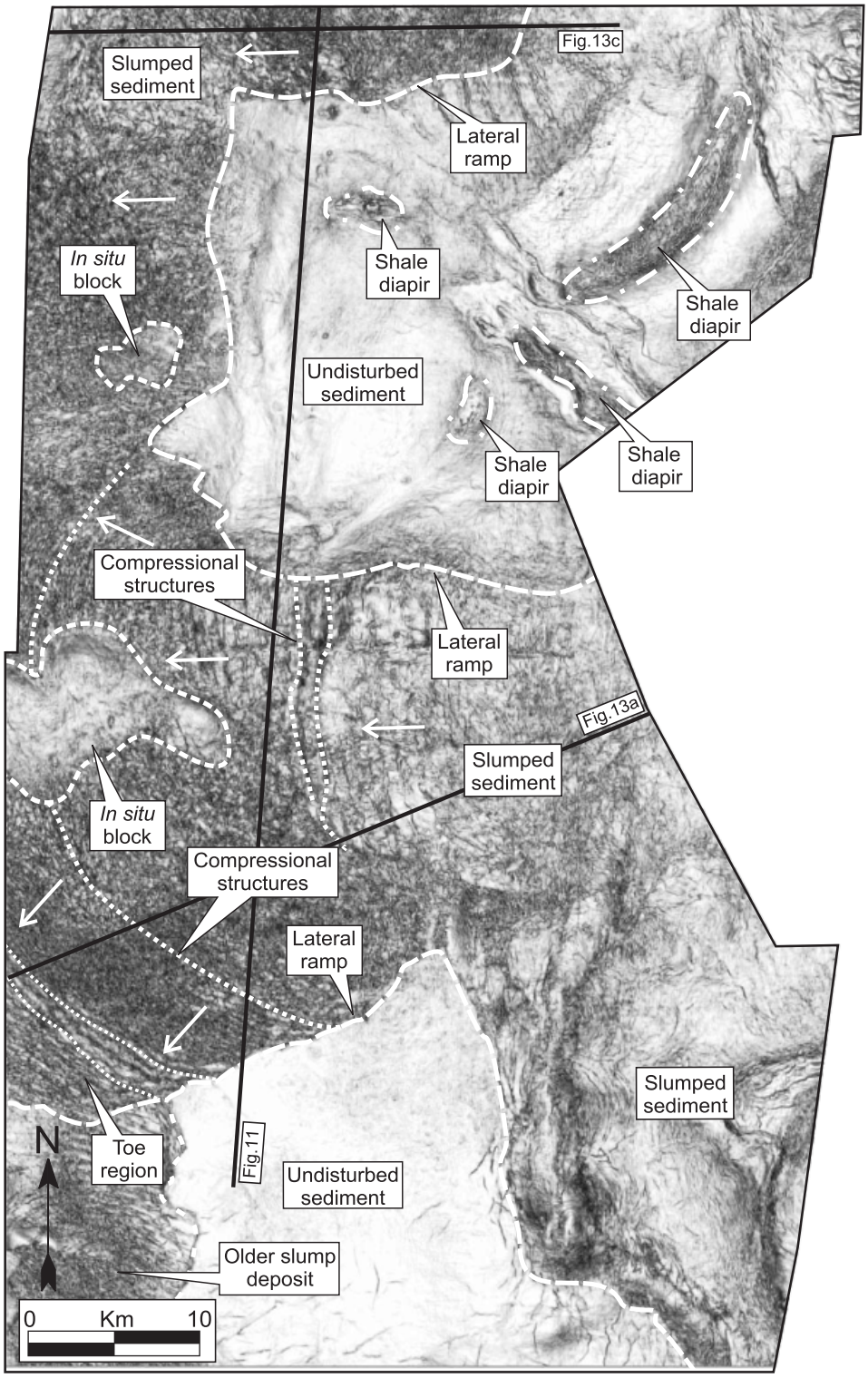

Fig. 12. Structurally flattened horizontal coherence-slice across the Levant 3D area (see Fig. 8 for location). The internal geometry of the lower region of the Israel Slump Complex is clearly observable. Sharp lateral ramps mark the limits of the slump mass. Note the contrast between the slumped and the undisturbed sediment and the presence of concentric arcs of ridge-like structures because of downslope compressional stress. *In situ* blocks of undisturbed sediments are observed. Arrows indicate the interpreted direction of transport of the slump mass.

accords well with the thickening of the slump body observed in the toe region (Fig. 10b).

The observed thrusts and fold systems are invaluable as kinematic indicators, and allow the direction and magnitude of translation of the slump mass to be constrained (e.g. Strachan, 2002). According to these compressional systems, a dominant eastern–western direction is observed within the overall downslope region of the ISC (Fig. 12). This direction accords well with the inferred down-palaeoslope trend and suggests a simple compressional regime. However, towards a lateral margin, the compressional lineations suggest a more complex situation with a dominant north-west–south-east direction. This variation may be indicative of a change in the kinematics of the slump mass as a result of compressional and frictional stress-regimes along the interfaces of the ISC.

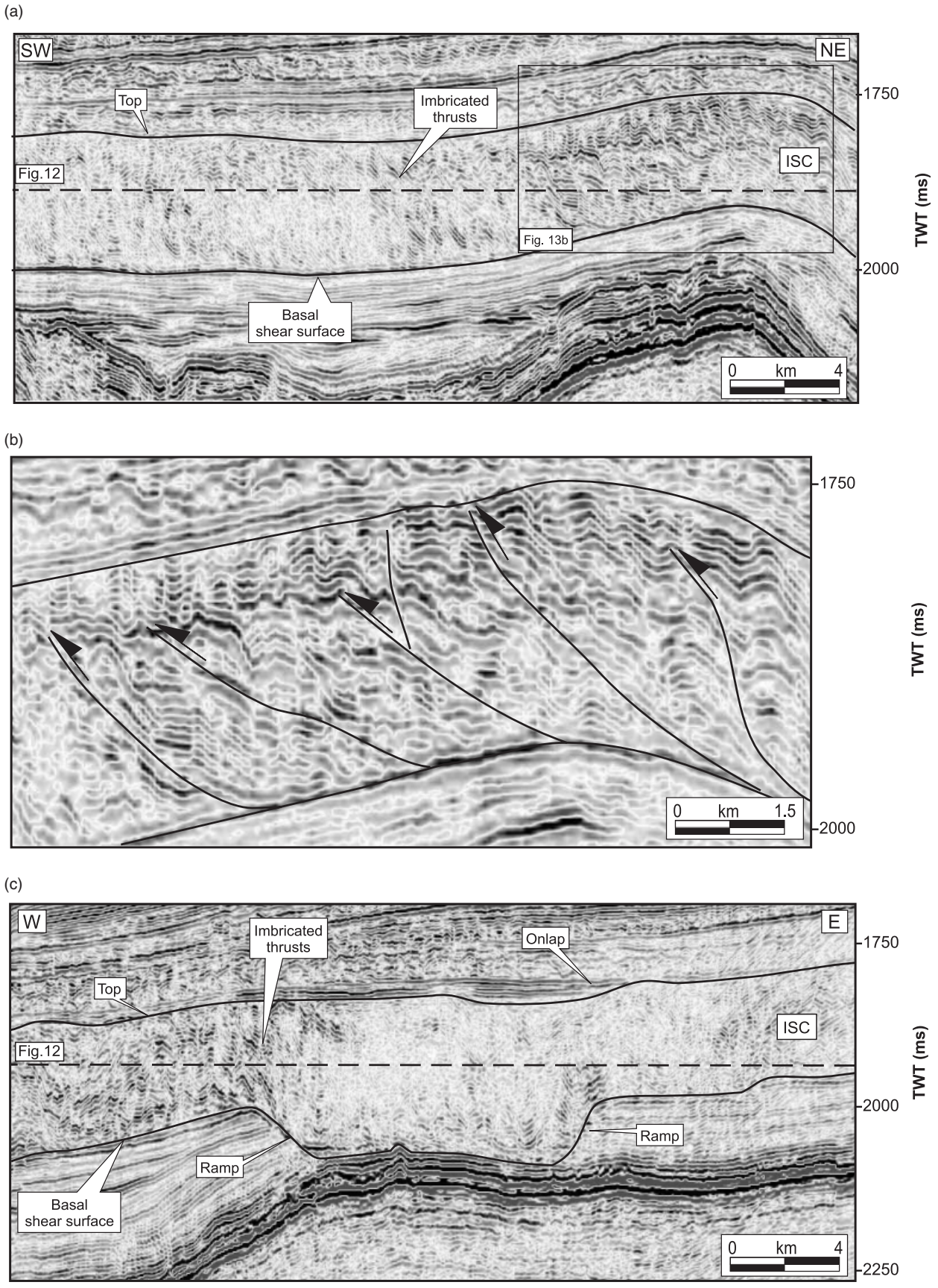

Fig. 13. Seismic examples of the internal geometries of the Israel Slump Complex (ISC) (see Fig. 12 for location). The direction of movement is north-east—south-west. (a) Dip seismic section showing imbricated series of closely spaced thrusts. (b) Enlargement of the section across a group of thrusts. Note that thrusts ramp up from the basal shear surface (see text for discussion). (c) Dip seismic section showing a large-scale ramp in the basal shear surface. Note the presence of imbricated thrusts propagating in the direction of movement and an onlapped depression.

Another important observation regarding the internal geometry of the ISC is that in certain areas, blocks of undisturbed and continuous seismic reflections remain as totally undeformed 'islands' surrounded by the highly deformed slump mass (Figs 11 and 12). These are remarkable in that they exhibit a laterally concordant and continuous seismic facies and are clearly coupled to the undeformed sedimentary succession below (Fig. 11). The blocks are separated from the surrounding slump body by steep outward dipping flanks of between 20° and 25° (Fig. 11).

These blocks could be interpreted as intact masses of sediment that have been translated as rafts within the more highly deformed slump mass. However, this interpretation can be discounted as a possibility, because their internal stratigraphy is clearly rooted to the strata directly below, and there is no visible detachment surface present at their base. An alternative interpretation that appears more plausible is that they represent isolated cores that have not experienced failure, and that the failed material propagated around them. This interpretation places significant constraints on the local kinematics of the slump mass surrounding these cores, and it is unlikely from this argument that large-scale translation could have occurred within these parts of the ISC.

Basal shear surface. The basal shear surface of the ISC forms a continuously traceable seismic reflection that separates the highly deformed seismic units within the slump body from the underlying and undeformed strata (Figs 9–11). On seismic profiles, it appears as a high-amplitude negative reflection that cuts up and down the stratigraphy in a staircase-like geometry (Fig. 11). Towards the headscarp region, the basal shear surface becomes increasingly steeper forming a concave upwards surface that cuts the overlying stratigraphic interval (Figs 9a and 10a). In the toe region, it steepens dramatically to form a frontal ramp (Fig. 10b). The lithology within the basal shear surface of the ISC is unknown; however, the significant acoustic impedance contrast suggests an abrupt lithologic or diagenetic contrast at this stratigraphic level.

Large-scale ramps (e.g. 80–90 m) that form indentations in the basal shear surface are recognised in several sectors of the ISC (Figs 9b and 11). These are most clearly delimited within the downslope parts of the ISC although their presence should not be ruled out in other areas where the resolution of the data is inferior. Seismic sections, both parallel and perpendicular to the main direction of slump movement, exhibit these ramps as conspicuous erosional features against which underlying seismic reflections are truncated. They have remarkably steep flanks that dip at between 20° and 25° and connect the deepest segments of the basal shear surface to shallower stratigraphic levels (Figs 11 and 13c). Above the ramps, the slump mass undergoes folding in order to accommodate the topographic gradient of the basal shear surface (Fig. 13c). We propose that these ramps are related to changes in the mechanical properties of the slumped material, the basal shear surface or the interaction of these factors.

In summary, the ISC constitutes a buried and buttressed large-scale slump complex within the Upper Pliocene succession. From the data available, we suggest that it is comprised of a minimum of three large-scale slump bodies, although smaller scale episodes of mass wasting should not be ruled out. A continuous basal shear surface that corresponds to a strong negative and continuous seismic reflection underlies the entire slump mass. This basal shear surface is affected by several ramps that form a staircase-like geometry. The ISC is divided into two main zones according to its seismic character. The first is located in a steep upslope region (ca. 6°) underlain by folded structures from the Syrian Arc system. This zone is characterised by extensional deformational structures (i.e. listric normal faults) and by thinning of the slump mass. Its upslope perimeter is well constrained by the presence of a continuously mapped headscarp. In this paper, this area is interpreted as the depletion zone of the ISC (*sensu* Varnes, 1978). The second zone is situated in a gentle (ca. 1°), downslope area that is underlain by thick accumulations of Messinian evaporites. This sector is dominated by compressional structures (i.e. folds and thrusts) and by thickening of the slump body. Its downslope limit is marked by the toe region. Blocks of undeformed seismic reflections that are rooted to the underlying strata and topographic ramps are locally observed. This area is interpreted as the accumulation zone of the ISC (*sensu* Varnes, 1978). The main features of the ISC are summarised in Fig. 14.

The GSC

The GSC is an array of three slump bodies observed on the present day seabed of the study area (Figs 7 and 15). Morphometric analysis of the seabed map combined with cross-sectional interpretation has led to the recognition of these three component slumps. Their cross-cutting relationships have been used to define the sequence of slumping events.

The GSC is located 40 km offshore from Gaza city, in a water depth ranging from 500 to 1150 m, with slope gradients between 2° and 0.5°, respectively. The failure zone trends north-westwards and covers an area of ca. 110 km^2 (mean length 22 km, mean width 5 km; Fig. 15b). The GSC affects up to 80 m of fine-grained claystones within Unit T10. It is, therefore, a moderately sized feature compared with other reported submarine slope instability products (e.g. Dingle, 1977; Bugge, 1983; Bugge *et al*., 1987).

Seismic character of the GSC

Headscarp. Three different headscarps are recognised within the GSC based on the abrupt offsets of the seabed topography (Figs 7 and 15b). Two of these (GSC-1, GSC-2) are clearly seen on the dipmap of the seabed (Fig. 15b). The GSC-1 is confirmed in seismic cross-sections (Fig. 16a) as a excisional feature, where there is an abrupt reduction of stratigraphic section in a downslope direction. The third headscarp within the GSC (GSC-3), is less

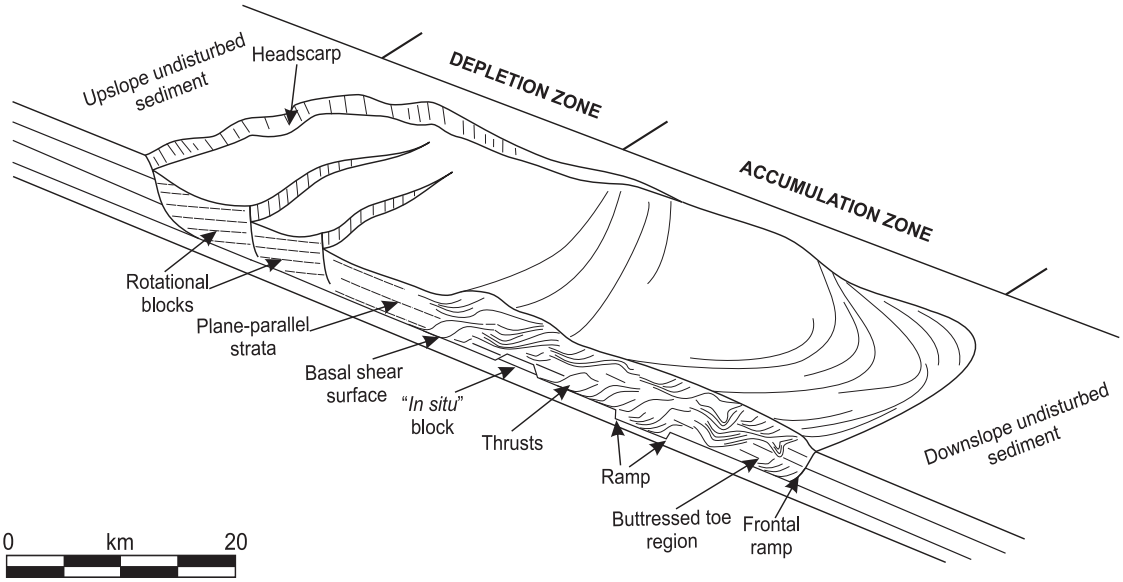

Fig. 14. Schematic depiction of part of the Israel Slump Complex. The upslope parts of the slump mass correspond to the depletion zone. This is characterised by extensional deformational structures and thinning of the slump mass. Note the presence of listric faults forming a series of rotational blocks that are tilted downslope. The downslope part of the slump body corresponds to the accumulation zone. This is characterised by compressional structures and thickening of the slump mass. The slump mass is buttressed against the downslope strata in the toe region. Note the presence of individual *in situ* blocks, which have been interpreted as indicators of a limited downslope displacement.

obvious on the dipmap (Fig. 15b), but is observable on the seismic profiles as an excisional scarp with ca. 10–20 m loss of stratigraphic section (Fig. 16a). The planform geometry of all three headscarps is crescentic, with either single salients (e.g. GSC-1 and GSC-3) or a double salient (e.g. GSC-2; Fig. 15a). Immediately downslope of the headscarps GSC-1 and GSC-2, there is a region of marked extensional thinning, where the slump bodies are cut by minor listric faults that have a distinct seabed scarp of up to 70 m height (Fig. 16a). The geometry of these faults bears a close relationship to the respective headscarps immediately updip, and are interpreted as retrogressive failure surfaces, that are widely recognised on other slump deposits (e.g. Evans *et al*., 1996; Mulder & Cochonat, 1996).

Upslope of the headscarp of GSC-1 is a region affected by elongated and subtle topographic depressions that are parallel to the headscarp and reach a length of ca. 4 km (Fig. 15). On seismic sections, these appear as small-scale faults and fractures that are locally coincident with larger-scale fault systems (Fig. 16a). By comparison with subaerial analogues (e.g. Farrell, 1984; Fitches *et al*., 1986; Martinsen & Bakken, 1990) and previous models for slump deposits (e.g. Varnes, 1978), these features are interpreted here as crown-cracks. Crown-cracks may form in the undisplaced material adjacent to the headscarp of a slump deposit as a result of development of extensional stresses by undermining and represent the upslope propagation of slumping during retrogressive failure.

The spatial distribution of the three main headscarps and their cross-cutting relationships are the major criteria to constrain the relative timing of the slump bodies within the GSC. A lateral margin of GSC-1 is clearly seen on Fig. 15b to be cross-cut by the headscarp of GSC-2. The headscarp of GSC-3 cuts into the seabed topography associated with both GSC-1 and GSC-2 in their combined toe region (Fig. 15b). The sequence of slumping is, therefore, interpreted to be GSC-1 followed by GSC-2 and finally GSC-3.

Toe. The toe regions of the three slumps forming the GSC are to a great extent overlapping and hence are difficult to distinguish. In a combined sense, the gross toe region for the entire GSC is recognised on the seabed dipmap as an area of intense rugosity (Fig. 15b), which in cross-section appears as short wavelength and low relief 'crumpling' of the seabed and the immediately underlying sections (Fig. 16a). The precise geometry of these topographic irregularities cannot be described in detail because of the limits of vertical and lateral resolution of the 3D seismic data. However, some of these 'crumples' have a ridge-like morphology that is evident on the seabed dipmap and are approximately arcuate in the downslope direction (Fig. 15b). These features are interpreted here as compressional ridges.

Seismic profiles across the toe region show the gross thickening within the GSC, with the resultant top surface of the slump body forming an irregular and elevated region above the level of the undeformed slope section (Fig. 16a and c). Downslope seismic profiles also show a frontal ramp where the basal shear surface climbs up section similarly to that described for the ISC (Fig. 16a). However, the GSC is not buttressed against the downslope strata as previously seen for the ISC (c.f. Fig. 10b). Instead, it overlies these strata for up to 2 km forming an interval of diffuse and very low amplitude seismic facies (Fig. 16a), with a

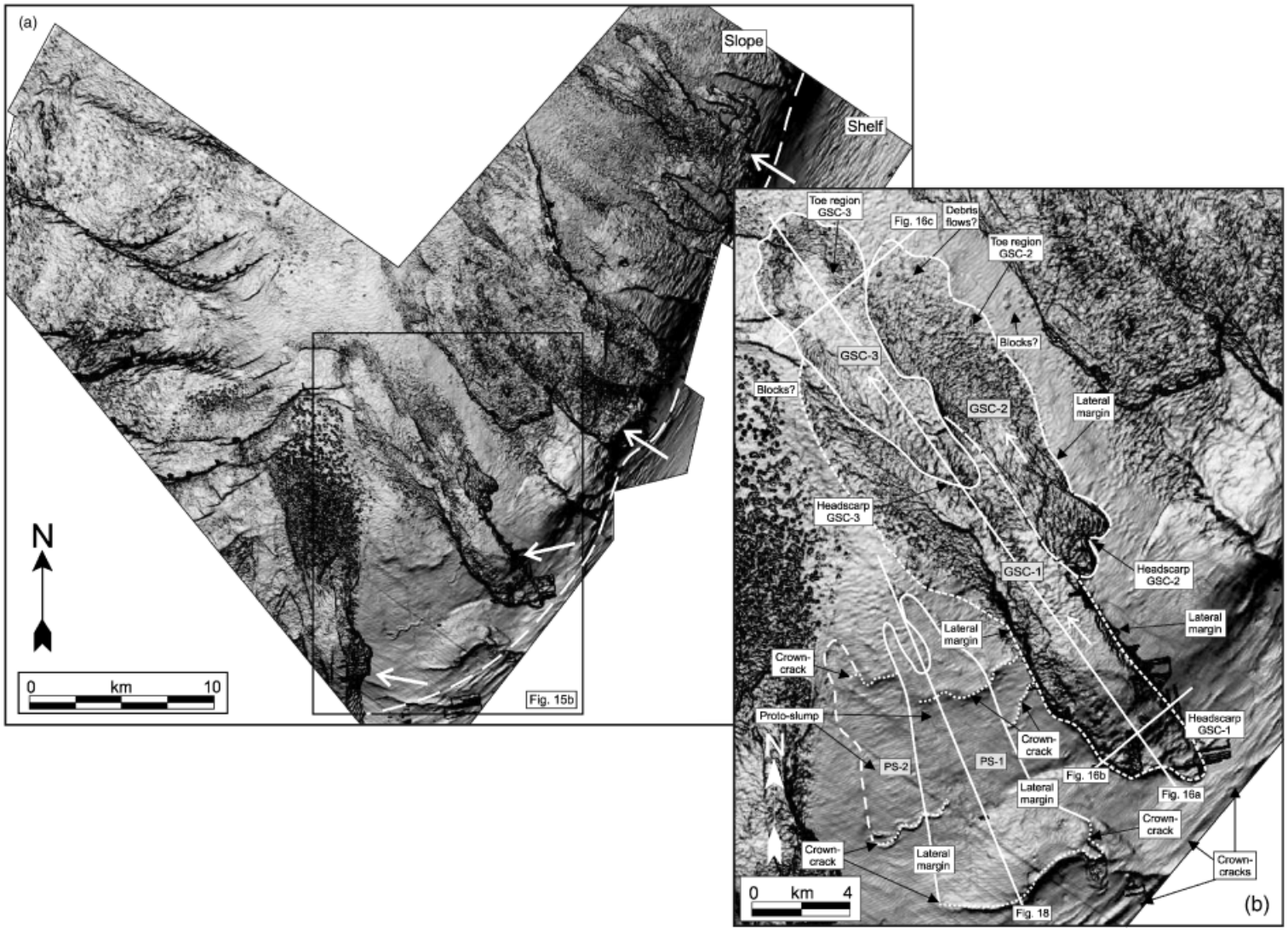

Fig. 15. Dip maps extracted from the present day seabed in the Levant 3D area. (a) Dip map showing the present-day shelf and slope. The dashed line represents the shelf-break. Four main arrays of slumps (marked by arrows) are observable. Note the marked headscarps located close to the shelf-break. Slump deposits create elongated bodies extending downslope. The box outlines the position of the Gaza Slump Complex (GSC). (b) Enlargement of the GSC. Note the presence of three clear headscarps suggesting a complex history of instability. The strike-parallel lineaments upslope of the headscarps GSC-1 and GSC-2 are interpreted as crown-cracks. Note the presence of two elongated bodies interpreted as proto-slumps (PS-1 and PS-2). The continuous straight lines indicate the position of seismic profiles used to illustrate the internal appearance of the GSC and the PS-1 (Figs 16 and 18, respectively).

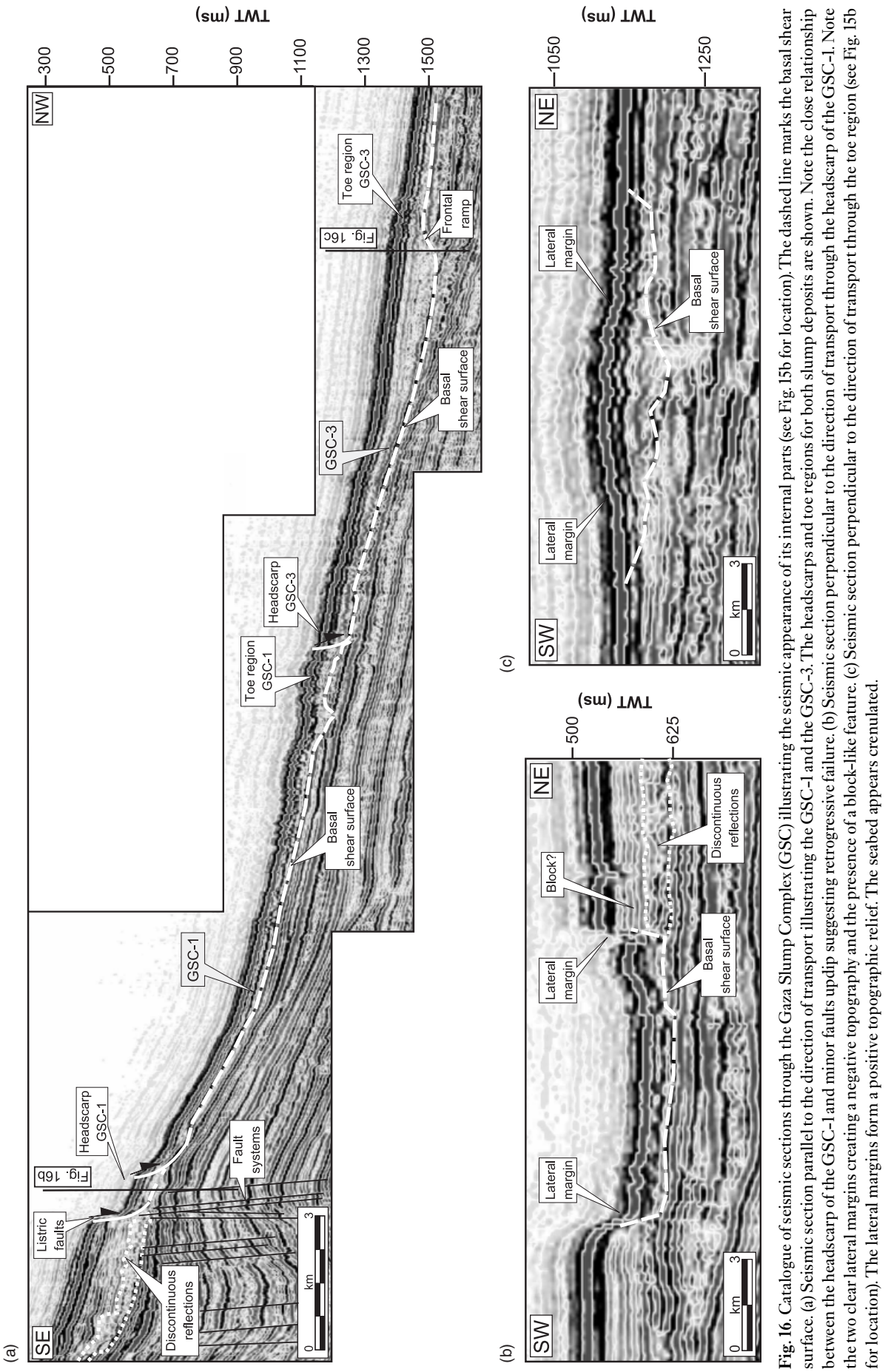

Fig. 16. Catalogue of seismic sections through the Gaza Slump Complex (GSC) illustrating the seismic appearance of its internal parts (see Fig. 15b for location). The dashed line marks the basal shear surface. (a) Seismic section parallel to the direction of transport illustrating the GSC-1 and the GSC-3. The headscarps and toe regions for both slump deposits are shown. Note the close relationship between the headscarp of the GSC-1 and minor faults updip suggesting retrogressive failure. (b) Seismic section perpendicular to the direction of transport through the headscarp of the GSC-1. Note the two clear lateral margins creating a negative topography and the presence of a block-like feature. (c) Seismic section perpendicular to the direction of transport through the toe region (see Fig. 15b for location). The lateral margins form a positive topographic relief. The seabed appears crenulated.

rather chaotic appearance in plan view (Fig. 15b). This interval is interpreted as block clusters and debris flow deposits derived from the toe regions of the GSC.

Lateral margins. Well-developed lateral margins are recognised along the flanks of all the three-component slumps within the GSC. In plan view, these lateral margins, together with the headscarps, define a chute-like slip domain, with an aspect ratio strongly elongated downslope, indicating a north-westwards gross slip direction (Fig. 15b). On seismic profiles, although the internal resolution of the slump deposits is poor, they can be seen to separate the undeformed slope sediments from the deformed units within the slump bodies (Fig. 16b and c). Their aspect varies from steep scarps in the upslope parts of the GSC (Fig. 16b), to smooth positive topographies downslope (Fig. 16c). Often, the steep scarps in the upslope areas are flanked by subparallel groups of smaller-scale fractures that define blocks of well-layered strata (Fig. 16b). These are interpreted as hanging blocks that might be metastable to rigid lateral collapse along the lateral margins.

Basal shear surfaces. Three different basal shear surfaces (one for each slump) can be correlated throughout the GSC. These are all defined as the lower boundary of the deformed and chaotic stratal seismic reflections within each slump body abutting against the undeformed underlying slope strata (e.g. Fig. 16). These basal shear surfaces are generally highly concordant with the underlying stratigraphy, except near the headscarps, where they cut up section and exhibit a listric geometry, and along the toe region, where they are seen to ramp downslope (Fig. 16a). The original lithology of the basal shear surfaces is unknown, because of the lack of petrophysical calibration of the shallow section in the available exploration wells. However, it is noteworthy, that all three basal shear surfaces correlate laterally with intervals of discontinuous and low amplitude seismic reflections (Fig. 16a, b). These intervals could be interpreted as a buried slump or slide deposits formed initially at the seabed. However, this is discounted as a possibility because they form continuously traceable intervals of constant thickness that are concordant with the surrounding strata throughout the study area and have no evidence of significant downslope displacement. Instead, we propose the interpretation that these intervals represent weak or incompetent layers because of loss of coherence in the sediment.

In summary, the GSC forms a medium-scale slump complex comprised by three simple slump deposits from the Late Pleistocene–Holocene. Each slump deposit consists of an upslope region characterised by gross volume loss and extensional structures, and a downslope region dominated by gross volume gain and compressional features (Fig. 17). These areas are interpreted here as the depletion and accumulation zones (*sensu* Varnes, 1978) of the GSC, respectively. The majority of extensional structures correspond to listric normal faults that die out on the basal shear surface and involve retrogressive failure. The compressional structures correspond to arcuate and compressional ridge-like geometries that propagate in the downslope direction (Fig. 17). The sequence of slumping within the GSC is interpreted to be GSC-1 followed by

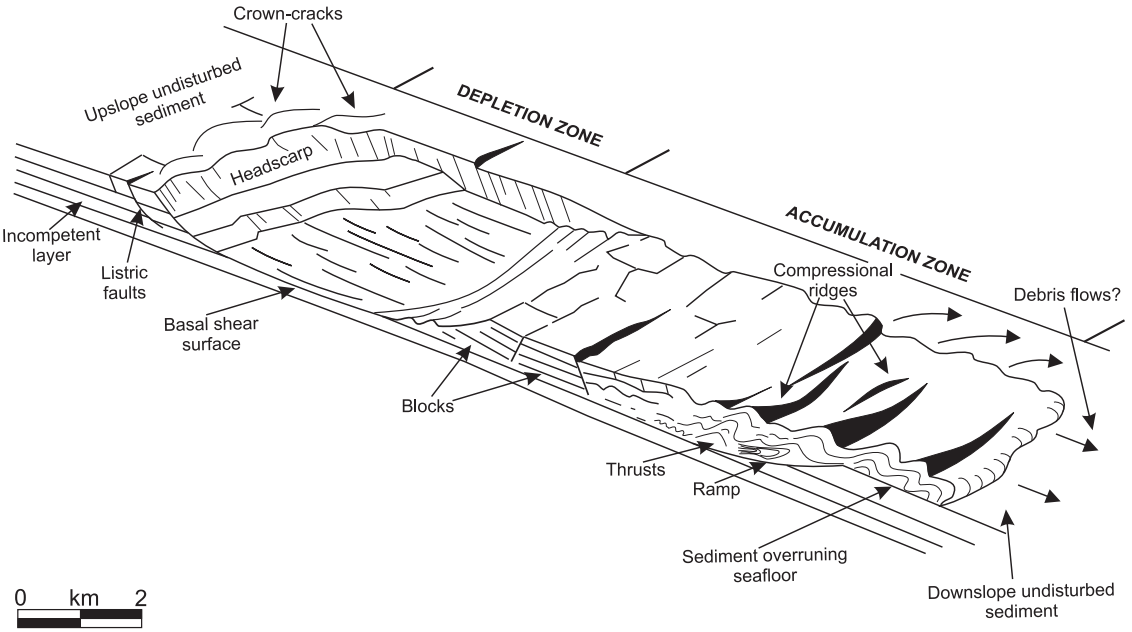

Fig. 17. Schematic depiction of part of the Gaza Slump Complex. The slump body is divided into two main parts: the depletion zone and the accumulation zone. The depletion zone shows a spoon-shaped depression suggesting reduction of the sediment column. Note the presence of a clear headscarp and evidences of retrogressive failure in the upslope parts. The accumulation zone is characterised by compressional structures and gain of material. In the toe region, the slumped material over runs the previous seabed. Inspired by O'Leary (1991).

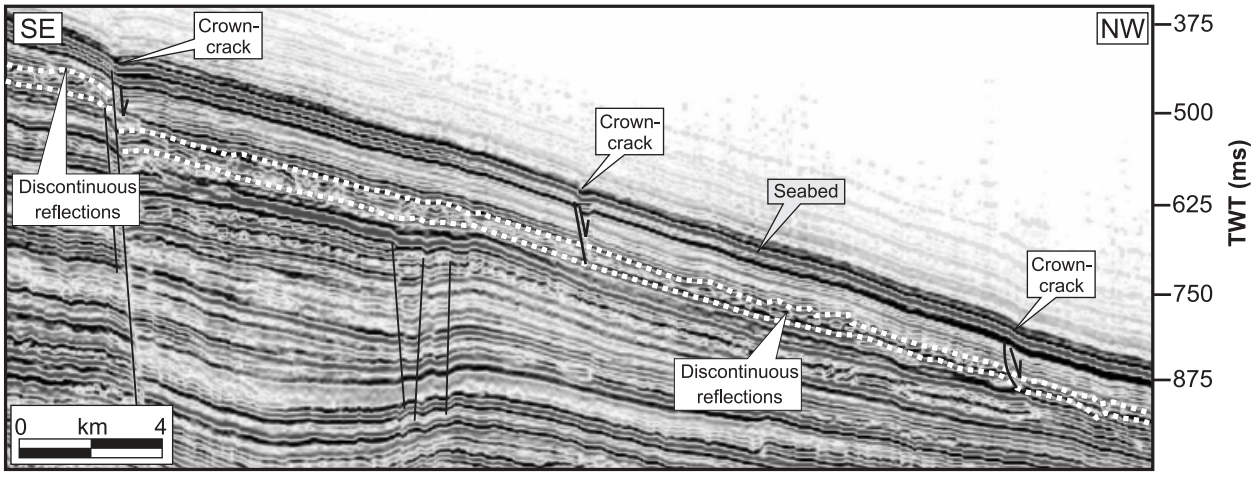

Fig. 18. Seismic profile through proto-slump-1 (PS-1) (see Fig. 15b for location). Note the small topographic depressions on the seabed interpreted as crown-cracks. These correspond to faults and fractures that are rooted in an interval of discontinuous seismic reflections interpreted here as an incompetent layer.

GSC-2 and GSC-3, respectively. This is a highly important observation as it implies that slump evolution within the GSC occurs by downslope propagation failure. Three different basal shear surfaces are identified within the GSC (one for each component slump). They all correlate laterally into intervals of discontinuous and low-amplitude seismic reflections that are interpreted here as incompetent layers characterised by loss of coherence in the sediment.

PROTO-SLUMPS

In this paper, a proto-slump is defined as the resulting product (as imaged on 3D seismic data) of an immature or failed stage of slumping. We consider proto-slumps to be the result of long-term strength degradation processes of dipping strata and the potential precursors to mass movement. Proto-slumps may display many of the diagnostic structures identified from slump deposits (e.g. lateral margins, crown-cracks). However, they lack a basal shear surface and clear extensional or compressional deformational structures, as their downslope displacement is highly restricted or absent.

In the study area, two main proto-slumps (PS-1 and PS-2) are observed in a region of the present day seabed that is not affected by slump deposits (Fig. 15b). In plan view, these proto-slumps appear as chute-like features that extend from the shelf-break to the mid-slope area with an aspect ratio strongly elongated in the downslope direction (Fig. 15b). The planforms of the PS-1 and PS-2 are defined by two groups of lineations that are parallel and perpendicular to the downslope direction (Fig. 15b). By analogy with the GSC, these lineations are interpreted as lateral margins and crown-cracks, respectively.

On seismic profiles, the PS-1 and PS-2 do not show a chaotic seismic facies as those described from slump deposits. Instead, they appear as intervals of slightly irregular, continuous and well-layered strata that overly a unit of discontinuous and medium-amplitude seismic reflections interpreted here as an incompetent layer (Fig. 18). Small-scale faults and fractures are the only deformational structures observed within the PS-1 and PS-2. These are rooted in the incompetent layer and are locally expressed on the seabed as small topographic depressions that correspond to the crown-cracks previously described (Fig. 18). No indication of loss or gain of material is observed in any part of the PS-1 and PS-2, which is compelling evidence to indicate a very restricted downslope displacement.

DISCUSSION

The most important observations undertaken from seismic interpretation of the slump complexes within the study dataset are summarised as follows:

1. Several discrete examples of medium- to large-scale slump complexes (ca. 40) have been identified within the Pliocene to Holocene succession of the Israeli continental margin.
2. In seismic profiles, these slump complexes appear as intervals of chaotic or highly disrupted seismic facies in sharp contrast with the laterally continuous and undeformed strata. They are bounded by an erosional basal shear surface and by a continuous and mounded top surface.
3. The majority of these slump complexes are composed of several (~3) discrete slump deposits of (approximately) the same order of magnitude.
4. Each slump deposit is divided into an upslope and a downslope region. The first is dominated by extensional deformational structures and thinning of the slump mass. The second is characterised by compressional structures and thickening of the slump mass.
5. Slump complexes are distributed along the entire post-Messinian Israeli margin and extend from the shelf to the base of slope areas. In the vertical sense, they tend to form sets of stacked bodies regularly interbedded with hemipelagic sediments.

6. There are distinct regions along the Israeli continental margin where slump complexes are concentrated. These are overlying large submarine canyon systems in the pre-Messinian section and structures from the Syrian Arc system.
7. There is a general increase in the number of slump bodies on moving up through the stratigraphy of the post-Messinian slope system within the southern parts of the study area. However, the volume of individual slump bodies clearly decreases upwards.
8. The ISC (Late Pliocene) is the oldest large-scale slump complex identified along the Israeli continental margin and involves large amounts of material (ca. 1000 km^3 in volume). It forms a buttressed slump body that is comprised by a minimum of three large-scale slump deposits.
9. The GSC (Late Pleistocene–Holocene) corresponds to a slump complex on the present day continental margin of Israel. It forms a medium-scale array of three slump deposits that exhibit evidence of upslope and downslope propagation failure.

The foregoing observations demonstrate that the entire post-Messinian continental margin of Israel is intrinsically affected by processes of slope instability. The most outstanding resultant elements are a series of large-scale slump complexes that extend from the shelf-break to the base of slope areas involving an average of ca. 15% of the total post-Messinian sediments. Analysis of their stratigraphic context in the southern continental margin has revealed that these slump deposits diminish in size and increase in number towards the shallowest intervals. It has also been shown that there are regions of the margin where slump deposits concentrate and the presence of a slump body influences the position of succeeding events. These regions correspond mainly to the parts of the margin overlaying regional structures from the Syrian Arc system or large pre-Messinian canyons (e.g. the Afiq and el-Arish submarine canyons).

Large-scale slumping initiated during the Late Pliocene with the ISC, which represents the largest slump complex in the region and is comparable with some of the biggest documented examples of submarine mass-wasting deposits in the world (i.e. Storegga Slide; Bugge, 1983). The most striking characteristic of the ISC is that the slump mass is clearly entrenched within the underlying strata (e.g. Figs 10b and 14). This is especially patent in its toe region where the ISC buttresses against the undisturbed sediments, which trap the slump mass preventing its movement farther downslope. This observation raises important implications for the mechanism and kinematics of movement and emplacement of the slump body. A detailed mechanical analysis of the ISC goes beyond the scope of this paper. However, from the previous observations, it is likely that the ISC resulted from a confined type of slumping that experienced a very limited downslope movement (ca. 5–15 km). The presence of blocks of undisturbed and continuous reflections that are coupled to the undeformed sedimentary succession corroborates this interpretation.

Previous investigators have reported other submarine mass-wasting deposits presenting this characteristic style of emplacement and have interpreted them as the result of quasi *in situ* deformation processes (e.g. Suvero Slide; Trincardi & Normark, 1989; Gela Slide; Trincardi & Argnami, 1990). The previous examples considered morphological obstacles as the main contributing factor for confinement of the respective slumped masses. In this paper, however, this is precluded as the cause for the entrenching of the ISC within the underlying sediments as the toe region is built in a near horizontal area where there is no morphological barrier able to create such a topographic confinement. Instead, we propose that a major contribution to the style of emplacement of the slumped mass resulted from relatively deep rooting of the basal shear surface within the underlying strata probably because of an abrupt lithological variation at that stratigraphic level combined with the general morphology of the strata.

Since the deposition of the ISC, slump events continued episodically up to the Holocene. As a result, tens of slump deposits and complexes formed at different stratigraphic levels interbedded with periods of normal hemipelagic deposition. The GSC is the most representative example of one of these slump complexes. It is located on the present day seabed of the study area and is composed of several different elements, resulting from an orderly sequence of linked slumping events. The overall resultant assemblage comprises three cross-cutting slump deposits that are interpreted as Late Pleistocene to Holocene in age. Each of these deposits includes an upslope area characterised by gross volume loss and extensional structures (depletion zone; Fig. 17), and a downslope region dominated by gross volume gain and compressional features (accumulation zone; Fig. 17). The architecture and geometry of each slump deposit indicate that slump evolution was controlled by a combination of retrogressive upslope and downslope propagation of failure. The relative ages of the three component deposits have been determined from their cross-cutting relationships, with the interpreted ordered sequence: GSC-1 followed by GSC-2 and GSC-3, respectively. Three basal shear surfaces, one associated with each component slump, have been observed and correlated with intervals of incompetent layers. This critical observation strongly suggests that movement in the GSC took place along surfaces of weakness and was controlled and limited by the number and distribution of these planes.

The occurrence of such a large number of slump deposits as that observed in the study area raises the obvious question of what internal or external factors predisposed the post-Messinian continental margin of Israel to be so susceptible to repeated failure. Previous studies have identified a number of possible causes controlling the development of submarine slump deposits along continental margins. These include:

- Destabilisation of gas hydrates (e.g. Andreassen *et al.*, 1990, Laberg & Vorren, 2000).

- Presence of gas in the sediments (e.g. Prior & Coleman, 1978; Carpenter, 1981; Duperret *et al*., 1995).
- High-sedimentation rates (e.g. Prior & Coleman, 1982; Aksu & Hiscott, 1989; Hiscott & Aksu, 1994, Laberg & Vorren, 2000; Imbo *et al*., 2002).
- Seismicity (e.g. Lewis, 1971; Dingle, 1977; Hampton *et al*., 1978; Prior & Coleman, 1984; Keefer, 1994; Hasiotis *et al*., 2002; Imbo *et al*., 2002).
- Steepening of slope angle (e.g. Martinsen, 1989; Hampton *et al*., 1996; Imbo *et al*., 2002).

In the case of the slump deposits presented here, the number of possible controlling factors is constrained by the available data. There is no evidence from seismic or well data of gas hydrates, which probably rules out this possibility as a controlling factor for slumping in the study area. However, abundant accumulations of biogenic gas within the post-Messinian succession have been revealed by the seismic and well data. Bubble-phase gas has the effect of increasing pore fluid pressures and hence reducing the effective normal stress on a potential slide plane, along with increasing its susceptibility to failure when stressed by earthquakes (Whelan *et al*., 1976; Barnes & Lewis, 1991). The presence of free gas could thus have played an important role in facilitating the mobilisation of sediments in the study area.

Rapid deposition because of high-sedimentation rates can result in underconsolidation of buried layers of clay-rich sediment in which upward hydraulic gradients reduce the internal shear strength of the sediment and lead to slope instability. The Pliocene–Quaternary section in the study area is up to 2-km thick with an average accumulation rate of about 0.5 mm yr^{-1}. According to these figures, the sedimentation rates are not likely to be sufficient to build up significant excess in pore pressure within these deposits in order to generate the observed large-scale slump deposits. However, the role of temporal variations in the sedimentation rates within the study area should not been discounted. During the Pliocene and Pleistocene period, the margin was affected by several episodes of global eustatic sea-level oscillations and local vertical tectonic movements that resulted in repeated transgressions and regressions (e.g. Almagor, 1993; Buchbinder & Zilberman, 1997). In such situations, sedimentation rates could have been considerably higher than the average rates, and could have thus facilitated mass-wasting processes.

The direct link between seismicity and instability of submarine slopes have been widely described in the literature (e.g. Lewis, 1971; Prior & Coleman, 1984; Edwards *et al*., 1993; Keefer, 1994; Hasiotis *et al*., 2002; Imbo *et al*., 2002). Earthquakes have two effects on the sediments of a slope system (Hampton *et al*., 1978). Firstly, violent earthquakes generate intermittent horizontal and vertical acceleration stresses that produce a direct loading on the sediment. Secondly, earthquakes can increase fluid pressure in the sediment that causes a reduction in the effective stress and therefore friction in the basal shear surface.

Because of its position at the zone of interaction between the Anatolian, African and Arabian plates, the continental margin of Israel is a seismically active region. Recent seismic activity in the area is presently concentrated in a broad zone off the coasts of Israel and Lebanon (Arieh, 1967) and along the Dead Sea Transform (Al-Tarazi, 1999). In the investigated area, the main seismic hazard is associated to the Syrian Arc system and the Dead Sea Transform, which is the result of a rifting process active in the region since the Miocene (e.g. Garfunkel, 1981; 1998).

Despite the importance of slope gradient in slope stability assessment (e.g. Hampton *et al*., 1996) our results show that occurrence of slope instability in the study area does not correspond with regionally increased slope gradients. The average slope angle within the post-Messinian succession is modest compared with many unstable slopes ($\alpha = 2–6^{\circ}$). Slopes are stable as long as the angle of internal friction (Φ) is greater than the slope angle (α). Considering a typical total angle of internal friction for a claystone of $\Phi = 15^{\circ}$, it is evident that the slope angles in the study area are not sufficient to cause large-scale instability under static gravitational loading alone. However, local increases in the slope angle appear to control the occurrence of slumping in specific areas. As previously argued, the majority of slump deposits within the study area are concentrated in regions underlain by regional structures from the Syrian Arc system and by pre-Messinian canyons. In these regions, locally accentuated slope angles occur ($\alpha = 5–6^{\circ}$). This concurrence might suggest a link between local oversteepening and higher occurrence of slope failure.

3D seismic interpretation has proved to be a very powerful tool for analysing slumping processes and results. It has provided excellent coverage of both recent and ancient slump deposits, allowing for a better understanding of their basinal distribution and geological setting. In addition, the higher spatial resolution provided by the 3D seismic data have offered a better definition of the basal shear surface of individual deposits, which is critical for unravelling the chronology of events within slump complexes. 3D seismic data have also allowed a greater understanding of the geometries (external and internal) and a more accurate volumetric analysis of slump deposits, which are critical aspects for modelling the kinematics and dynamics of slumping processes. The value of 3D seismic data as a tool for submarine slope instability risk assessment has also been proved in this paper. An interesting aspect of this approach is the possibility to map the extent of zones where diagnostic features of mass movement (i.e. proto-slumps) can be inferred, thus highlighting potential areas affected by slope instability. It must be emphasised, however, that the nature of the data has allowed for identification of only medium to large-scale slump deposits and proto-slumps, but unresolvable small-scale features most probably also exist throughout the study area.

CONCLUSIONS

1. Slumping is an intrinsic facet of the slope system of the Israeli continental margin from the Early Pliocene to the present day.
2. Simple and complex slump deposits occur at many different stratigraphic levels within the post-Messinian succession of the Israeli continental margin.
3. Large-scale slumping in the Israeli continental margin commenced in the Late Pliocene with the ISC, which is one of the largest slumps in the world (ca. 1000 km^3 in volume) described to date.
4. Since then, slumping processes repeatedly occurred up to the Holocene. Slumping events increased in number through time although the resulting products decreased in size.
5. The high occurrence of slumping processes was possible because of a combination of seismic activity, presence of gas within the sediments and slope oversteepening. The degree of interaction between these triggering mechanisms may have varied through time.
6. Evidence of potential slope instability occurring in the future in the study area is indicated by the presence of proto-slumps.
7. 3D seismic interpretation has proved to be a powerful tool when analysing slump processes and results. The availability of a 3D understanding of slump deposits is critical to evaluate the geological context and architectural elements of slump deposits. From this geometrical foundation, many aspects related to the mechanics, processes and controlling factors of slumping seem likely to be inferred.

ACKNOWLEDGMENTS

The authors are indebted to BG-Group for making the seismic and well data available and for their permission to publish the interpretation of the data. We are also grateful to Schlumberger GeoQuest for use of IESX and GeoViz software. Zvi Garfunkel, Paul Spencer and Lorna Strachan are thanked for their reviews of the manuscript which led to significant improvements. D. James is greatly acknowledged for his detailed and constructive comments and thoughtful critiques. Thanks are due to R. Davies, S. Maddox, V. P. Wright, A. Robinson and C. Bertoni for suggesting editing improvements to the manuscript. Finally, we are very grateful for the technical support we have received from N. S. Ferguson.

REFERENCES

Aksu, A.E. & Hiscott, R.N. (1989) Slides and debris flows on the high-latitude continental slopes of Baffin Bay. *Geology*, **17**, 885–888.

Almagor, G. (1980) Halokinetic deep-seated slumping on the Mediterranean slope of northern Sinai and southern Israel. *Mar. Geotech.*, **4**, 83–105.

Almagor, G. (1984) Salt-controlled slumping on the Mediterranean slope of central Israel. *Mar. Geophys. Res. Lett.*, **6**, 227–243.

Almagor, G. (1986) Mass transport on the continental slope of Israel. *Geo-Mar. Lett.*, **6**, 29–34.

Almagor, G. (1993) Continental slope processes off northern Israel and southernmost Lebanon and their relation to onshore tectonics. *Mar. Geol.*, **112**, 151–169.

Almagor, G. & Schilman, B. (1995) Sedimentary structures and sediment transport across the continental slope of Israel from piston core studies. *Sedimentology*, **42**, 575–592.

Almagor, G. & Wiseman, G. (1977) Analysis of submarine slumping in the continental slope off the southern coast of Israel. *Mar. Geotech.*, **2**, 349–388.

Al-tarazi, E.A. (1999) Regional seismic hazard study for the eastern Mediterranean (Trans-Jordan, Levant and Antakia) and Sinai region. *J. Afr. Earth Sci.*, **28**, 743–750.

Andreassen, K., Hogstad, K. & Berteussen, K.A. (1990) Gas hydrate in the southern Barents Sea, indicated by shallow seismic anomaly. *First Break*, **8**, 235–245.

Arieh, E. (1967) Seismicity of Israel and adjacent areas. *Geol. Surv. Isr. Bull.*, **43**, 1–4.

Barnes, P.M. & Lewis, K.B. (1991) Sheet slides and rotational failures on a convergent margin: the Kidnappers Slide, New Zealand. *Sedimentology*, **38**, 235–245.

Ben-Avraham, Z. (1989) The structure and tectonic setting of the Levant continental margin-eastern Mediterranean. *Tectonophysics*, **8**, 351–362.

Bøe, R., Hovland, M., Instanes, A., Rise, L. & Vasshus, S. (2000) Submarine slide scars and mass movements in Karmsundet and Skudenesfjorden, southwestern Norway: morphology and evolution. *Mar. Geol.*, **167**, 147–165.

Booth, J.S. & O'leary, D.W. (1991) A statistical overview of mass movement characteristics on the North American Atlantic outer continental margin. *Mar. Geotech.*, **10**, 1–18.

Brown, L.F. & Fisher, W.L. (1977) Seismic–stratigraphic interpretation of depositional systems: examples from Brazilian rift and pull-apart basins. In: *Seismic Stratigraphy – Applications to Hydrocarbon Exploration* (Ed. by C.E. Payton), *AAPG Mem.*, **26**, 213–248.

Buchbinder, B. & Zilberman, E. (1997) Sequence stratigraphy of Miocene–Pliocene carbonate-siliciclastic shelf deposits in the eastern Mediterranean margin (Israel): effects of eustasy and tectonics. *Sediment. Geol.*, **112**, 7–32.

Bugge, T. (1983) Submarine slides on the Norwegian continental margin, with special emphasis on the Storegga area. *Cont. Shelf Inst. Publ.*, **110**, 152.

Bugge, T., Befring, S., Balderson, R.H., Eidvin, T., Eystein, J., Kenyon, N.H., Holtedahl, H. & Sejrup, H.P. (1987) A giant three-stage submarine slide off Norway. *Geo-Mar. Lett.*, **7**, 191–198.

Carpenter, G. (1981) Coincident sediment slump/clathrate complexes on the U.S. Atlantic continental slope. *Geo-Mar. Lett.*, **1**, 29–32.

Dingle, R.V. (1977) The anatomy of a large submarine slump on a sheared continental margin (SE Africa). *J. Geol. Soc. London*, **134**, 293–310.

Druckman, Y., Buchbinder, B., Martinotti, G.M., Siman Tov, R. & Aharon, P. (1995) The buried Afiq Canyon (eastern Mediterranean, Israel): a case study of a Tertiary submarine canyon exposed in Late Messinian times. *Mar. Geol.*, **123**, 167–185.

Duperret, A., Bourgois, J., Lagabrielle, Y. & Suess, E. (1995) Slope instabilities at an active continental margin:

large-scale polyphase submarine slide along the northern Peruvian margin, between 5°S and 6°S. *Mar. Geol.*, **122**, 303–328.

Edwards, B.D., Lee, H.J. & Field, M.F. (1993) Seismically induced mudflow in Santa Barbara Basin, California. In: *Submarine Landslides: Selected Studies in the U.S. Exclusive Economic Zone* (Ed. by W.C. Schwab, H.J. Lee & D.C. Twichell), *U.S. Geol. Surv. Bull.*, **2002**, 167–175.

Embley, R.W. (1980) The role of mass transport in the distribution and character of deep ocean sediments with special reference to the North Atlantic. *Mar. Geol.*, **38**, 23–50.

Embley, R.W. & Jacobi, R. (1977) Distribution and morphology of large submarine sediment slides and slumps on the Atlantic continental margins. *Mar. Geotech.*, **2**, 205–208.

Evans, D., King, E.L., Kenyon, N.H., Brett, C. & Wallis, D. (1996) Evidence for long-term instability in the Storegga Slide region off western Norway. *Mar. Geol.*, **130**, 281–292.

Eyal, Y. (1996) Stress field fluctuations along the Dead-Sea Rift since the Middle Miocene. *Tectonics*, **15**, 157–170.

Farrell, S.G. (1984) A dislocation model applied to slump structures, Ainsa Basin, South Central Pyrenees. *J. Struct. Geol.*, **6**, 727–736.

Field, M.E. & Barber, J.H. (1993) A submarine landslide associated with shallow seafloor gas hydrates off northern California. In: *Submarine Landslides: Selected Studies in the U.S. Exclusive Economic Zone* (Ed. by W.C. Schwab, H.J. Lee & D.C. Twichell), *U.S. Geol. Surv. Bull.*, **2002**, 151–157.

Field, M.E., Gardner, J.V., Jennings, A. E. & Edwards, B.D. (1982) Earthquake-induced sediment failures on a 0.25° slope, Klamath River delta, California. *Geology*, **10**, 542–546.

Fitches, W.R., Cave, R., Craig, J. & Maltman, A.J. (1986) Early veins as evidence of detachment in the Lower Palaeozoic rocks of the Welsh Basin. *J. Struct. Geol.*, **8**, 607–620.

Frydman, S., Wiseman, G. & Almagor, G. (1982) Effects of earthquakes on slope stability, continental shelf of Israel. *GSI Curr. Res.*, 66–71.

Garfunkel, Z. (1981) Internal structure of the Dead Sea leaky transform (rift) and its relations to plate kinematics. *Tectonophysics*, **80**, 81–108.

Garfunkel, Z. (1984) Large-scale submarine rotational slumps and growth faults in the eastern Mediterranean. *Mar. Geol.*, **55**, 305–324.

Garfunkel, Z. (1998) Constrains on the origin and history of the Eastern Mediterranean basin. *Tectonophysics*, **298**, 5–35.

Garfunkel, Z. & Almagor, G. (1985) Geology and structure of the continental margin off northern Israel and the adjacent part of the Levantine Basin. *Mar. Geol.*, **62**, 105–131.

Garfunkel, Z. & Almagor, G. (1987) Active salt dome development in the Levant basin, southeast Mediterranean. In: *Dynamical Geology of Salt Related Structures* (Ed. by I. Lerche & J. O'Brien), pp. 263–300. Academic Press, New York.

Garfunkel, Z., Arad, A., Bugge, T. & Almagor, G. (1979) The Palmahin Disturbance and its regional setting. *Geol. Surv. Isr. Bull.*, **72**, 56pp.

Garfunkel, Z. & Derin, B. (1984) Permian-Early Mesozoic tectonism and continental margin formation of Israel and its implications for the history of the eastern Mediterranean. In: *The Geologic Evolution of the Eastern Mediterranean* (Ed. by J.E. Dixon & A.H.F. Robertson), pp. 187–201. Blackwell Scientific Publications, Boston, MA.

Hampton, M.A., Bouma, A.H., Carlson, P.R., Molnia, B.F., Clukey, E.C. & Sangrey, D.A. (1978) Quantitative study of slope instability in the Gulf of Alaska. *10th Annual Offshore Technology Conference (OTC)*, **4**, 2307–2318.

Hampton, M.A., Lee, H.J. & Locat, J. (1996) Submarine landslides. *Rev. Geophys.*, **34**, 33–59.

Hasiotis, T., Papatheodorou, G., Bouckovalas, G., Corbau, C. & Ferentinos, G. (2002) Earthquake-induced coastal sediment instabilities in the western Gulf of Corinth, Greece. *Mar. Geol.*, **3100**, 1–17.

Hiscott, R.N. & Aksu, A.E. (1994) Submarine debris flows and continental slope evolution in front of Quaternary ice sheets, Baffin Bay, Canadian Arctic. *AAPG Bull.*, **78**, 445–460.

Hsü, K.J., Montadert, L., Bernoulli, D., Cita, M.B., Erikson, A., Garrison, R.G., Kidd, R.B., Meliers, F., Muller, C. & Wright, R. (1978) History of the Mediterranean salinity crisis. *Init. Rep. DSDP*, **42A**, 153–1078.

Imbo, Y., De Batist, M., Canals, M., Prieto, M.J. & Baraza, J. (2002) The gebra slide: a submarine slide on the Trinity Peninsula Margin, Antarctica. *Mar. Geol.*, **3259**, 1–18.

Jansen, E., Befring, S., Bugge, T., Eidvin, T., Holtedahl, H. & Sejrup, H.P. (1987) Large submarine slides on the Norwegian continental margin: sediments, transport and timing. *Mar. Geol.*, **78**, 77–107.

Keefer, D.K. (1994) The importance of earthquake-induced landslides to long-term slope erosion and slope-failure hazards in seismically active regions. *Geomorphology*, **10**, 265–284.

Kenyon, N.H. (1987) Mass-wasting features on the continental slope of northwest Europe. *Mar. Geol.*, **74**, 57–77.

Knebel, H. & Carson, B. (1979) Small-scale slump deposits, middle Atlantic Continental Slope, off eastern United States. *Mar. Geol.*, **29**, 221–236.

Laberg, J.S. & Vorren, T.O. (2000) The Trænadjupet Slide, offshore Norway-morphology, evacuation and triggering mechanisms. *Mar. Geol.*, **171**, 95–114.

Lee, H.J., Locat, J., Dartnell, P., Israel, K. & Wong, F. (1999) Regional variability of slope stability: application to the Eel margin, California. *Mar. Geol.*, **154**, 305–321.

Lee, H.J., Schwab, W.C., Edwards, B.D. & Kayen, R.E. (1991) Quantitative controls on submarine slope failure morphology. *Mar. Geotech.*, **10**, 143–157.

Lee, H.J., Syvitski, J.P.M., Parker, G., Orange, D., Locat, J., Hutton, E.W.H & Imram, J. (2002) Distinguishing sediment waves from slope failure deposits: field examples, including the 'Humboldt slide', and modelling results. *Mar. Geol.*, **192**, 79–104.

Lewis, K.B. (1971) Slumping on a continental slope inclined at 1°–4°. *Sedimentology*, **16**, 97–110.

Locat, J. & Lee, H. (2002) Submarine landslides: advances and challenges. *Can. Geotech. J.*, **39**, 193–212.

Martinsen, O.J. (1989) Styles of soft-sediment deformation on a Namurian (Carboniferous) delta slope, western Irish Namurian Basin, Ireland. In: *Deltas: Sites and Traps for Fossil Fuels* (Ed. by M.K.G. Whateley & K.T. Pickering), *Spec. Publ. Geol. Soc. London*, **41**, 167–177.

Martinsen, O.J. & Bakken, B. (1990) Extensional and compressional zones in slumps and slides in the Namurian of County Clare, Ireland. *J. Geol. Soc. London*, **147**, 153–164.

McAdoo, B.G., Pratson, L.F. & Orange, D.L. (2000) Submarine landslide geomorphology, U.S. continental slope. *Mar. Geol.*, **169**, 103–136.

Moore, D.G., Curray, J.R. & Emmel, F.J. (1976) Large submarine slide (olistostrome) associated with Sunda Arc subduction zone, northeast Indian Ocean. *Mar. Geol.*, **21**, 211–226.

Moore, J.G., Clague, D.A., Holcomb, R.T., Lipman, P.W., Normark, W.R & Torresan, M.E. (1989) Prodigious

submarine landslides on the Hawaiian Ridge. *J. Geophys. Res.*, **94**(B12), 17465–17484.

Montadert, L., Letouzey, J. & Mauffret, A. (1978) Messinian event: seismic evidence. *Init. Reports DSDP*, **42**, 1032–1050.

Moore, J.G., Normark, W.R. & Holcomb, R.T. (1994a) Giant Hawaiian landslides. *Annu. Rev. Earth Planet. Sci.*, **22**, 119–144.

Moore, J.G., Normark, W.R. & Holcomb, R.T. (1994b) Giant Hawaiian underwater landslides. *Science*, **264**, 46–47.

Mulder, T. & Cochonat, H.P. (1996) Classification of offshore mass movements. *J. Sediment. Res.*, **66**, 43–57.

Nardin, T.R., Hein, F.J., Gorsline, D.S. & Edwards, B.D. (1979) A review of mass movement processes and acoustic characteristics, and contrasts in slope and base-of-slope system versus canyon–fan–basin floor systems. In: *Geology of Continental Slopes: Society of Economic Paleontologists and Mineralogists Special Publication*, **Vol. 27** (Ed. by L.J. Doyle & O.H. Pilkey), pp. 61–73. SEPM, Tulsa, OK.

Normark, W.R. & Gutmacher, C.E. (1988) Sur submarine slide, Monterey Fan, central California. *Sedimentology*, **35**, 629–647.

O'Leary, D.W. (1991) Structure and morphology of submarine slab slides: clues to origin and behaviour. *Mar. Geotech.*, **10**, 53–69.

O'Leary, D.W. (1993) Submarine mass movement, a formative process of passive continental margins: the Munsen–Nygren landslide complex and the southeast New England landslide complex. In: *Submarine Landslides: Selected Studies in the U.S. Exclusive Economic Zone* (Ed by W.C. Schwab, H.J. Lee & D.C. Twichell), *U.S. Geol. Surv. Bull.*, **2002**, 23–39.

Prior, D.B., Bornhold, B.D. & Johns, M.W. (1984) Depositional characteristics of a submarine debris flow. *J. Geol.*, **92**, 707–727.

Prior, D.B. & Coleman, J.M. (1978) Submarine landslides on the Mississippi River Delta-front slope. *Geosci. Man*, **19**, 41–53.

Prior, D.B. & Coleman, J.M. (1979) Submarine landslides – Geometry and nomenclature. *Geomorphol. N. F.*, **23**, 415–426.

Prior, D.B. & Coleman, J.M. (1982) Active slides and flows in underconsolidated marine sediments on the slopes of the Mississippi Delta. In: *Workshop on Marine Slides and Other Mass Movements. NATO Conference Series IV* (Ed. by S. Saxov & J. Nieuwenhuis), pp. 225–234. Plenum Press, New York.

Prior, D.B. & Coleman, J.M. (1984) Submarine slope instability. In: *Slope Instability* (Ed. by D. Brundsen & D.B. Prior), pp. 419–455. Wiley, Chichester, New York.

Sivan, D., Gvirtzman, G. & Sass, E. (1999) Quaternary stratigraphy and paleogeography of the Galilee coastal plain, Israel. *Quat. Res.*, **51**, 280–294.

Smith, J.R., Malahoff, A. & Shor, A.N. (1999) Submarine geology of the Hilina slump and morpho-structural evolution of Kilauea volcano, Hawaii. *J. Volcanol. Geotherm. Res.*, **94**, 59–88.

Stow, D.A.A. (1986) Deep clastic seas. In: *Sedimentary Environment and Facies*, 2nd edn (Ed. by H.G. Reading), pp. 399–444. Blackwell Scientific Publications, Oxford.

Strachan, L. (2002) Slump-initiated and controlled syndepositional sandstone remobilisation: an example from the Namurian of County Clare, Ireland. *Sedimentology*, **49**, 25–41.

Trincardi, F. & Argnami, A. (1990) Gela Submarine slide: a major basin-wide event in the Plio–Quaternary foredeep of Sicily. *Geo-Mar. Lett.*, **10**, 13–21.

Trincardi, F. & Normark, W.R. (1989) Sediment waves on the Tiber prodelta slope: interaction of deltaic sedimentation and currents along the shelf. *Geo-Mar. Lett.*, **8**, 149–157.

Tibor, G. & Ben-Avraham, Z. (1992) Late Tertiary seismic facies and structures of the Levant passive margin off central Israel. *Mar. Geol.*, **105**, 253–273.

Varnes, D.J. (1978) Slope movement types and processes. In: *Landslides, Analysis and Control. Special Report*, **176** (Ed. by R.L. Schuster & R.J. Krizek), pp. 11–33. National Academy of Sciences, Washington.

Watts, A.B. & Masson, D.G. (1995) A giant landslide on the north flank of Tenerife, Canary Islands. *J. Geophys. Res.*, **100**(B12), 24487–24498.

Whelan, T.A., Coleman, J.M. & Suyayda, J.N. (1976) The geochemistry of recent Mississippi river delta sediments: gas concentration and sediment stability. Paper 94. *Offshore Technology Conference*, Texas, pp. 71–84.

Woodcock, N.H. (1979) Sizes of submarine slides and their significance. *J. Struct. Geol.*, **1**, 137–142.

Received 8 December 2003; accepted: 10 July 2004.

